

Semiconductor Radiation Physics: From Defects to Devices

Final Report Prepared for

Gerald L. Witt
AFOSR/NE
801 North Randolph Street, Room 732
Arlington, VA 22203

Vanderbilt University MURI Program
Electrical Engineering and Computer Science Department
Box 1608, Station B
Nashville, TN 37235

Contract # F49620-99-1-0289
April 7, 2005

DISTRIBUTION STATEMENT A
Approved for Public Release
Distribution Unlimited

20050427 034

ENGINEERING REPORT DATA SHEET

 DISTRIBUTION UNLIMITED
 PROPRIETARY
 EXPORT CONTROLLED (ITAR)

The Institute for Space and Defense Electronics (ISDE) is a unit of Vanderbilt University, Nashville, TN, a not-for-profit higher-education research institution. Material contained herein should be deemed PROPRIETARY unless explicitly stated DISTRIBUTION UNLIMITED above. All requests for this document should be directed to the address in field 11 below. Direct all distribution inquiries to POC in field 20 below.

| | | | | | |
|--------------------|---------|------------------|-------------|----------------|------------------|
| 1. TRACKING NUMBER | 2. DATE | 3. CONTRACT NO. | 4. TASK NO. | 5. DELIVERABLE | 6. INTERIM/FINAL |
| F49620-99-1-0289 | 4/7/05 | F49620-99-1-0289 | | Report | Final |

| | | |
|------------------|--|--|
| 7. PROJECT TITLE | Vanderbilt University MURI Program | 10. TASK DESCRIPTION: Final Report submitted to summarize findings of MURI Program. |
| 8. TASK TITLE | Final Report | |
| 9. REPORT TITLE | Semiconductor Radiation Physics: From Defects to Devices | |

| | |
|--|---------------------------------|
| 11. ORGANIZATION NAME AND ADDRESS Institute for Space and Defense Electronics, Vanderbilt University 2014 Broadway, Suite 200, Nashville, Tennessee, 37203 | 12. PROJECT SPONSOR AFOSR/NE |
|--|---------------------------------|

| | | |
|--|---|-------------------------------|
| 13. TASK TECHNICAL POC Ron Schrimpf, Director | 14. E-MAIL ron.schrimpf@vanderbilt.edu | 15. TELEPHONE 615-343-0507 |
|--|---|-------------------------------|

| | | | |
|---------------------|-------------------|-----------------------------|------------|
| 16. TASK START DATE | 17. TASK DUE DATE | 18. REVISED COMPLETION DATE | 19. REASON |
| | | | |

| | | |
|---|---|-------------------------------|
| 20. TASK MANAGEMENT POC Ron Schrimpf, Director | 21. E-MAIL ron.schrimpf@vanderbilt.edu | 22. TELEPHONE 615-343-6677 |
|---|---|-------------------------------|

23. ISDE CLASSIFICATIONS / CATALOGING

| | | | | | |
|-----------|------------|-----------|---------------|-------------|--------------|
| 23A. TECH | 23B. MODEL | 23C. TOOL | 23D. ANALYSIS | 23E. DESIGN | 23F. INFRAST |
| | | | | | |

24. RELATED PROJECTS OR DOCUMENTS

| | | |
|--------------|-------|----|
| 25. KEYWORDS | PAGES | 54 |
| | | |

26. SYNOPSIS

Radiation effects have been a serious problem for electronics used in defense and space systems for decades and radiation-hardened devices, circuits, and systems have been developed to meet the needs of these systems. However, many of the fundamental physical mechanisms responsible for radiation-induced degradation were not elucidated, which limits the ability to extend the hardening methods to future generations of technology. This MURI program combined recently developed atomic-scale computational techniques and physical-analysis tools with an engineering approach to analyzing radiation effects in electronics. The computational work focused on using density functional theory to understand problems such as the enhanced low dose rate sensitivity of irradiated bipolar junction transistors and the fundamental mechanisms responsible for interface-trap formation. Several experimental techniques, including second harmonic generation and cathodoluminescence spectroscopy, were adapted to analyzing radiation-induced defects. The radiation response of advanced technologies, including GaAs- and GaN-based transistors, vertical cavity surface emitting lasers, and ultrathin dielectrics, was evaluated experimentally. All of these technologies appear promising for use in future defense and space systems.

WARNING - If the "ITAR" boxed is checked above, this document contains technical data whose export is restricted by the Arms Export Control Act (Title 22, U.S.C., Sec 2751, et seq.) or the Export Administration Act of 1979, as amended, (Title 50, U.S.C., App. 2401 et seq.) Violators of these export laws are subject to severe criminal penalties. Disseminate in accordance with provisions of DoD Directive 5230.25. Further dissemination only as directed.

Table of Contents

| | | |
|----------|--|-----------|
| 1 | OBJECTIVES | 1 |
| 2 | STATUS OF THE EFFORT..... | 3 |
| 3 | ACCOMPLISHMENTS/NEW FINDINGS | 5 |
| 3.1 | Defects and 1/f Noise in SiO ₂ | 5 |
| 3.2 | Radiation Effects and NBTI in High-K Dielectrics | 5 |
| 3.2.1 | <i>Heavy-Ion Induced Dielectric Breakdown.....</i> | 5 |
| 3.2.2 | <i>Radiation Effects in Hf Silicate and Alumina Dielectrics.....</i> | 5 |
| 3.2.3 | <i>1/f Noise in MOSFETS with High-K Gate Dielectrics.....</i> | 6 |
| 3.2.4 | <i>Negative Bias-Temperature Instability.....</i> | 6 |
| 3.3 | Theoretical Analysis of Radiation-Induced Defects | 7 |
| 3.4 | Contactless Characterization of Radiation-Induced Defects Using Intense, Tunable, Ultra-fast Laser Techniques | 13 |
| 3.5 | Characterization of Radiation Defects in Microelectronic Structures Using Physical and Electrical Characterization Techniques..... | 17 |
| 3.5.1 | <i>Objectives (Ohio State).....</i> | 17 |
| 3.5.2 | <i>Final Status of the Effort (Ohio State).....</i> | 17 |
| 3.5.3 | <i>Accomplishments/New Findings</i> | 20 |
| 3.6 | Proton Irradiation Effects on III – V Compound Semiconductor Devices | 21 |
| 3.7 | Proton Radiation Effect in Stripe Lasers and Vertical Cavity Surface Emitting Lasers (VCSELs)..... | 22 |
| 3.7.1 | <i>Objectives.....</i> | 22 |
| 3.7.2 | <i>Status of Effort.....</i> | 22 |
| 3.7.3 | <i>Accomplishments/New Findings (Program Summary).....</i> | 23 |
| 3.8 | Electronic Structure and Interface Properties of High-k Dielectric Gate Stacks in Advanced Si Devices..... | 24 |
| 3.8.1 | <i>Interface properties for Si devices</i> | 24 |
| 3.8.2 | <i>Electronic Structure of High-K Dielectrics</i> | 25 |
| 3.8.3 | <i>Scaling of Si Devices with High-K Gate Dielectrics</i> | 28 |
| 3.8.4 | <i>Gate Stacks for GaN Devices.....</i> | 28 |
| 3.9 | Defect Characterization in Advanced Semiconductor Devices | 29 |
| 3.9.1 | <i>Annealing Rate of the Luminescence W-Center in Silicon</i> | 29 |
| 3.9.2 | <i>Electron Ionization Damage in Ultrathin Zirconium Dielectrics.....</i> | 30 |
| 3.9.3 | <i>Defects Related to Nitrogen Sublattice Damage in Electron Irradiated GaN.....</i> | 31 |
| 3.9.4 | <i>Evaluation of Radiation Hardness of GaN.....</i> | 33 |
| 3.9.5 | <i>Radiation Tolerance of GaAs-On-Insulator MESFETs.....</i> | 34 |
| 3.9.6 | <i>Radiation Effects in AlGaIn/GaN Heterostructure Transistors</i> | 37 |
| 4 | PERSONNEL SUPPORTED..... | 39 |
| 5 | PUBLICATIONS..... | 41 |

Table of Contents (continued)

| | | |
|----------|---|-----------|
| 6 | INTERACTIONS/TRANSITIONS..... | 49 |
| 7 | NEW DISCOVERIES, INVENTIONS OR PATENT DISCLOSURES..... | 50 |
| 8 | HONORS/AWARDS | 51 |

List of Figures

| | | |
|----------------------|---|----|
| Figure 3.3.1: | Experimental, analytical and simulated interface trap density as a function of dose rate for an Analog Devices' RF25 capacitor irradiated to a total dose of 200 krad(SiO ₂). | 9 |
| Figure 3.3.2: | The concentration of neutralized acceptors as a function of irradiation bias voltage in a p-doped Si layer (solid line) compared with experiment (open circles). | 10 |
| Figure 3.3.3: | ΔN_{it} , ΔN_{bt} , and ΔN_{ot} estimated from the "dual-transistor border-trap" (DTBT) technique for annealing temperatures of 80 °C (upper panel) and 150 °C (lower panel). These devices were irradiated to 45 krad(SiO ₂) at 6 V with 10-keV x rays at a dose rate of 240 rad(SiO ₂), prior to annealing. [After D. M. Fleetwood et al., IEEE Trans. Nucl. Sci., 44, 1698 (1995)]. | 11 |
| Figure 3.3.4: | Interface-trap density as a function of time, temperature, and bias voltage. The solid line corresponds to T = 80 °C, the dashed line to T = 150 °C. | 12 |
| Figure 3.4.1: | The order of electron injection process from Si into SiO ₂ versus pump photon energy. | 14 |
| Figure 3.4.2: | Exponential fits of time-dependent SHG signals from the thick part of the oxide layer (left – injection; right – recombination). | 15 |
| Figure 3.4.3: | Exponential fits of time-dependent SHG signals from the thin part of the oxide layer (left – injection; right – recombination). | 15 |
| Figure 3.4.4: | Time-dependent SHG signal from a Si film with applied DC bias across the BOX. The inset figure shows electrical characteristics from direct probing. | 16 |
| Figure 3.9.1: | Photoluminescence spectra of silicon irradiated with 55 MeV protons to a fluence of 5×10^{11} cm ⁻² . Three different materials with largely different oxygen content are compared after 15 min annealing at 160°C. | 29 |
| Figure 3.9.2: | Annealing rate of the W-line compared at two different proton doses. The data have been normalized with respect to the luminescence intensity of the line after the 160C annealing step. | 30 |
| Figure 3.9.3: | RILC of Zr-based ultrathin dielectrics. | 31 |
| Figure 3.9.4: | Time-integrated luminescence spectra of the 250 μ m free-standing Samsung HVPE GaN before and after 0.42MeV electron irradiation. | 32 |

Table of Contents (concluded)

List of Figures (concluded)

| | |
|--|----|
| Figure 3.9.5: Time-integrated PL spectra after annealing. All spectra were measured at 11K, 10mW and with 4 seconds laser exposure. | 33 |
| Figure 3.9.6: Comparison of lifetime degradation constants K_t between GaN and GaAs. | 34 |
| Figure 3.9.7: Variation of the drain current I_d , transconductance g_m , and threshold voltage V_t with 55 MeV proton irradiation fluence for GaAs-On-Insulator and conventional MESFETs. | 35 |
| Figure 3.9.8: Fluence dependence of 1/f noise component for GaAs-On-Insulator and conventional MESFETs. | 37 |
| Figure 3.9.9: Current-voltage (IV) and capacitance-voltage (CV) characteristics of the gate diode of an AlGaIn/GaN heterostructure transistor before and after exposure to 55 MeV protons. | 38 |

List of Tables

| | |
|---|----|
| Table 3.9.1: Lifetime degradation constants for different GaN layers irradiated with 25 and 55 MeV protons. | 33 |
|---|----|

1 OBJECTIVES

This report documents work conducted as part of a five-year Multi-disciplinary University Research Initiative (MURI) in the area of Semiconductor Radiation Physics. Participating universities were Vanderbilt University, the University of Arizona, the University of California-Berkeley, North Carolina State University, and Ohio State University.

The primary objective of this program was to study the effects of radiation on silicon-based microelectronics and compound semiconductor-based optoelectronics. The thrust areas of this program were:

- i) Studying the electronic and atomic dynamics resulting from radiation to understand defect nucleation, defect evolution and growth, and defect reactions on the atomic scale;
- ii) Coupling the effects of radiation-induced defect interactions to device radiation response; and
- iii) Developing and validate engineering models, suitable for implementation in commercial TCAD tools that track these processes on a macroscopic scale.

The research was conducted at Vanderbilt University, Ohio State University, North Carolina State University, the University of California-Berkeley, and the University of Arizona. This report covers the five-year duration of the program.

It is essential to understand radiation effects in advanced space and defense systems that utilize highly scaled devices, very thin dielectrics, and advanced optoelectronics. Electronics deployed in these systems may be exposed to various forms of radiation, including energetic particles and high-energy photons. Development of physically-based testing and hardness-assurance techniques is essential to ensure that commercial off-the-shelf (COTS) parts used in military and space systems survive in the radiation environments in which they are deployed. It is particularly important to understand the physical mechanisms responsible for radiation-induced degradation as advanced technologies move into regimes in which new phenomena, such as quantum-mechanical effects and non-local transport, dominate device behavior. In recent years, significant progress has been made to understand the structure of defects and interfaces in semiconductors and insulators. In this program, we have applied some of these advanced computational and experimental techniques to study radiation effects in microelectronics.

At Vanderbilt University, the research involved the Departments of Electrical Engineering and Computer Science (EECS) and Physics. Within EECS, the work emphasized electrical measurements and models related to total-dose damage, electrical reliability, and single-event dielectric rupture in gate dielectrics and field oxides. In addition, experimental characterization of proton-induced defects in compound-semiconductor devices was performed in collaboration with other MURI participants. In Physics, the work focused on atomic-level modeling of defects in semiconductors and insulators and optical characterization of radiation-induced defects.

Researchers at North Carolina State University worked on alternative high-k gate dielectrics for advanced silicon and compound semiconductor devices. The primary objectives were to:

- i) Establish a science base for understanding the bulk and interface properties of high-k gate dielectrics for advanced silicon-based devices,
- ii) Narrow the field of potential high-k gate dielectric alternatives,
- iii) Identify intrinsic mechanisms that limit performance and reliability, including issues with respect to Moore's law scaling, and
- iv) Provide MOS devices with advanced high-k gate dielectrics to other team members for radiation testing.

Under sponsorship from the Office of Naval Research, the Air Force Office of Scientific Research, and the Semiconductor Research Corporation, these high-k gate dielectric materials were subjected to additional theoretical and experimental studies.

At Ohio State University, researchers probed the energies, densities, and spatial distributions of radiation-induced traps in MOSFETs, capacitors, and HEMTs using lateral and depth-resolved cathodoluminescence spectroscopy (CLS), spatially-resolved Secondary Ion Mass Spectrometry (SIMS), and a complement of electrical and electronic characterization probes of device parameters. In the context of the overall MURI, their goal was to identify physical mechanisms underlying formation of radiation-induced defects and methods to mitigate such effects via novel materials and processing. These measurements allowed correlation of electronic performance with the deep trap levels of AlGaN/GaN HEMTs and GaN Schottky barriers over a wide range of irradiation fluences.

At the University of California–Berkeley, research activities within the framework of the MURI focused on native point defects in advanced semiconductors. The main goal was to identify radiation-induced defects at the microscopic level and correlate the defect characteristics to the change of the material properties and device parameters.

The research objectives at the University of Arizona for this effort primarily focused on understanding the device physics and the implications of proton irradiations on both stripe and vertical cavity semiconductor lasers through modeling and simulation studies. This modeling activity also extended to system-level simulation in multi-physics optoelectronic systems.

2 STATUS OF THE EFFORT

This final report describes work conducted over the five-year duration of the program.

New models of oxygen vacancies in silicon dioxide were developed based on density functional theory calculations. Defects that were four-fold coordinated and five-fold coordinated were investigated. The dynamics of the charge exchange were found to be consistent with conditions under which significant $1/f$ noise is observed in MOS transistors. $1/f$ noise in back-gate silicon-on-insulator (SOI) MOS transistors was studied in detail and compared with shallow electron trapping in Si implanted buried oxides. Extensive studies of heavy-ion-induced breakdown of thin SiO_2 and high-k dielectrics were also carried out. High-k dielectrics were observed to be more resistant to heavy-ion-induced gate rupture than SiO_2 because of the greater physical thickness of the dielectrics. These studies, combined with the radiation tolerance studies indicate that high-k dielectrics could be introduced into future technologies for space applications. We also studied the negative bias temperature instabilities (NBTI) in high-k dielectrics. It was observed that effective activation energies of oxide and interface-traps are consistent with hydrogen models of NBTI.

Detailed calculations to understand the mechanisms controlling the atomic arrangement at the Si- SiO_2 interface were carried out. It was seen that an abrupt and smooth interface is energetically preferred. The reactions of hydrogen atoms and ions at Si- SiO_2 interfaces were also studied using density functional theory (DFT). It was also observed that H^+ is the only stable charge state of hydrogen at the Si- SiO_2 interface and that the energetically most stable configuration for oxygen and water in amorphous silica is an interstitial molecule. We also studied the enhanced low dose rate sensitivity (ELDRS) and radiation induced acceptor deactivation in bipolar devices.

Second Harmonic Generation (SHG) was examined as a non-invasive tool to probe buried interfaces. We developed a contactless two-color optical technique to monitor carrier transport by multiphoton internal-photoemission induced second harmonic generation. We were able to measure the Si- SiO_2 band offset and radiation induced carrier transport in thin SiO_2 using this technique. We also employed SHG to monitor interface quality and carrier dynamics in Si/ SiO_2 /Si (SOI) interfaces.

At Ohio State University, the energies, densities and spatial distributions of radiation induced traps in MOS devices and HEMTs were investigated using low energy electron-excited luminescence spectroscopy (LEEN), depth-resolved cathodoluminescence spectroscopy (CLS), spatially-resolved secondary ion mass spectroscopy (SIMS) and a number of other physical and electrical probes. The group at Ohio State concentrated on investigating the physical mechanisms underlying the formation of radiation induced defects and methods to mitigate these effects through novel materials and processing. Ultra-thin film dielectrics and radiation hard GaN-based devices were observed to be suitable for applications in radiation environments.

We studied GaN-based High Electron Mobility Transistors (HEMTs) for their radiation tolerance over the course of the MURI program. We found that AlGaIn/GaN and AlGaIn/AlN/GaN devices show excellent radiation tolerance, continuing to function up to a proton fluence of 10^{14} cm^{-2} . The device degradation was observed to be due to a decrease in the carrier mobility in the channel, a decrease in the sheet carrier density, changes in the Schottky barrier height and an

increase in the resistance of the thin film structure. Degradation in carrier density in the two-dimensional electron gas and deterioration of carrier mobility appear to be the dominant degradation mechanisms in these devices. Radiation effects in compound semiconductors, i.e., HEMTs and the Schottky diodes, were studied in collaboration with the researchers at the University of California, Santa Barbara. Overall, the gallium-nitride-based technologies examined appear to be very resistant to radiation, suggesting that they are good candidates for use in space systems.

The research efforts at University of Arizona focused on the study of radiation effects on optical and optoelectronic components and systems. The primary goal was to understand the basic physics and the effects of proton irradiation on stripe and vertical cavity semiconductor lasers. Extensive modeling and simulation efforts were undertaken to achieve this goal. The modeling studies were validated by experimental studies of these parts. Another goal was to extend the device-level models to the system level. To achieve this goal, a library of optical and optoelectronic component models was developed. These models could be used to study various optoelectronic systems exposed to various types of radiation.

The research effort at the North Carolina State University focused on the study of high-k dielectrics. The interface properties of aggressively scaled CMOS devices containing high-k dielectrics in the gate stack were studied. The band-edge electronic structures of high-k gate dielectrics containing transition metal and trivalent lanthanide rare earths were also studied. These studies were carried out using X-ray and UV spectroscopy. The bias-dependent trapping in these dielectrics was found to be consistent with the published results. In addition to gate stacks for Si devices, gate stacks for gallium nitride devices were also studied.

At University of California, Berkeley, the luminescence w-center in proton irradiated silicon was studied to understand its annealing behavior. Zr-based dielectrics were exposed to electron irradiations to study the radiation-induced leakage currents (RILC) in these dielectrics. Electron irradiations were also carried out on GaN to understand the radiation-induced damage to the nitrogen sublattice. The Berkeley group also studied proton damage effects in GaAs-on-insulator (GOI) MESFETs and AlGaIn/GaN HEMTs.

3 ACCOMPLISHMENTS/NEW FINDINGS

3.1 Defects and $1/f$ Noise in SiO_2

We developed new models of O vacancies in SiO_2 based on density functional theory calculations. Two types of defects were investigated – one that was fourfold coordinated that could form a stable dipole upon first hole and then electron capture, and one that was fivefold coordinated that could not form a dipole. The dynamics of charge exchange with these defects and with E_{δ} centers were found to be consistent with the known conditions under which one sees significant $1/f$ noise in MOS transistors. This is one of the very few physical systems now for which the defect dynamics of the underlying physical processes that cause $1/f$ noise are known to any significant degree. A unified model was developed that self-consistently describes $1/f$ noise, charge trapping and detrapping, and thermally stimulated current in SiO_2 ¹.

$1/f$ noise was studied in detail in back-gate SOI MOS transistors, and compared with shallow electron trapping observed in Si implanted buried oxides. It was found that Si implantation increased the back-gate noise of these devices, but further increases of the noise with irradiation were not seen. It was also found that the noise of some SOI devices could be understood within the framework of the Dutta-Horn Model, but in other cases, changes in the defect population during the device measurements were observed. This work will be important for understanding the performance and reliability of future double-gate devices, in which noise at the Si to buried oxide interface will become increasingly important².

3.2 Radiation Effects and NBTI in High-K Dielectrics

3.2.1 Heavy-Ion Induced Dielectric Breakdown

We performed extensive studies of heavy-ion-induced breakdown of thin SiO_2 and high-K dielectrics. We found that, owing to the greater physical thickness of the insulators, high-K dielectrics of sufficient quality to be useful for device application are more resistant to heavy ion induced gate rupture than their SiO_2 counterparts with similar effective oxide thicknesses. A model was developed for heavy ion induced degradation and failure that was based on the percolation model of oxide breakdown^{3,4}.

3.2.2 Radiation Effects in Hf Silicate and Alumina Dielectrics

Hafnium silicate capacitors with 4.5 nm equivalent oxide thickness gate insulators were irradiated with 10-keV x-rays. The midgap and flatband voltage shifts in these devices were found to increase linearly with dose and are significantly larger than the shifts seen in high quality, thermal SiO_2 gate oxides of similar electrical thickness. The standard radiation-induced charge trapping efficiency equation was adapted for calculating effective trapping efficiencies in alternative dielectrics and used to compare the radiation response of hafnium silicate to SiO_2 from several manufacturers. The effects of common reliability screens such as “burn-in” and bias stress tests were also

¹ D. M. Fleetwood, H. D. Xiong, Z. Y. Lu, et al., IEEE Trans. Nucl. Sci., vol. 49, pp. 2674 – 2683, 2002.

² H. D. Xiong, b. Jun, D. M. Fleetwood, et al., IEEE Trans. Nucl. Sci., vol. 51, pp. 3238 – 3242, 2004.

³ L. W. Messengill, B. K. Choi, D. M. Fleetwood, et al., IEEE Trans. Nucl. Sci., vol. 48, pp. 1904 – 1912, 2001.

⁴ B. K. Choi, D. M. Fleetwood, R. D. Schrimpf, et al., IEEE Trans. Nucl. Sci., vol. 49, pp. 3045 – 3050, 2002.

investigated. The radiation responses of these devices, coupled with the demonstrated resistance of these films to heavy-ion induced gate rupture in previous studies, suggest that alternative dielectrics to SiO₂ potentially could be integrated into future electronics technologies for many low-power space applications⁵.

We also examined the total-dose radiation response of capacitors and transistors with stacked Al₂O₃ on oxynitride gate dielectrics with Al and poly-Si gates after irradiation with 10 keV X-rays. The midgap voltage shift increased monotonically with dose and depended strongly on both Al₂O₃ and silicon oxynitride thickness. The thinnest dielectrics, of most interest to industry, are extremely hard to ionizing irradiation, exhibiting only ~ 50 mV of shift at a total dose of 10 Mrad(SiO₂) for the worst case bias condition. Oxygen anneals were found to improve the total dose radiation response by ~ 50 % and induce a small amount of capacitance-voltage hysteresis. Al₂O₃/ silicon oxynitride dielectrics that receive a ~ 1000 ° C dopant activation anneal trap ~ 12 % more of the initial charge than films annealed at 550°C. Charge pumping measurements show that the interface-trap density decreases with dose up to 500 krad(SiO₂). This surprising result is discussed with respect to hydrogen effects in alternative dielectric materials, and may be the result of radiation-induced hydrogen passivation of some of the near-interfacial defects in these gate dielectrics⁶.

3.2.3 1/f Noise in MOSFETS with High-K Gate Dielectrics

Low-frequency noise and irradiation response were studied for n-channel Metal-Oxide-Semiconductor Field-Effect Transistors (MOSFETs) with Al₂O₃/SiO_xN_y/Si(100) gate stacks. Radiation-induced threshold-voltage shifts and low-frequency noise were found to increase with dose and decrease with post-irradiation annealing. The border (near interfacial-oxide) trap density in the gate dielectric inferred from the noise measurements was significantly higher than that typically observed in thermal SiO₂. Similarly, the effective radiation-induced-hole trapping efficiency in Al₂O₃ gate dielectrics was significantly higher than for SiO₂ gate dielectrics of comparable thickness. The low-frequency noise in these high-κ devices could be described well by a number fluctuation model⁷.

3.2.4 Negative Bias-Temperature Instability

We have compared NBTI in MOS capacitors with SiO_xN_y/HfO₂ gate dielectrics to those with thermal SiO₂ oxides. Effective activation energies for interface and oxide-trap charge densities for each device type, estimated from capacitance-voltage measurements versus temperature and electric field, are found to lie in the range, 0.2 to 0.4 eV. These results are consistent with hydrogen models of NBTI, and support reaction-diffusion mechanisms⁸.

⁵ J. A. Felix, D. M. Fleetwood, R. D. Schrimpf, et al., IEEE Trans. Nucl. Sci., vol. 49, pp. 3191 – 3196, 2002.

⁶ J. A. Felix, M. R. Shaneyfelt, D. M. Fleetwood, et al., IEEE Trans. Nucl. Sci., vol. 50, pp 1910 – 1918, 2003.

⁷ H. D. Xiong, D. M. Fleetwood, J. A. Felix, et al., Appl. Phys. Lett., vol. 83, pp. 5232 – 5234, 2003.

⁸ X. J. Zhou, L. Tsetseris, S. N. Rashkeev, et al., Appl. Phys. Lett., vol. 84, pp. 4394 – 4396, 2004.

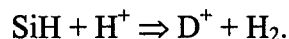
3.3 Theoretical Analysis of Radiation-Induced Defects

We used first-principles quantum-mechanical calculations, in combination with engineering analysis, to understand several key issues related to radiation-induced defects in semiconductor devices. These results are summarized briefly here.

Preferred atomic arrangements at a Si-SiO₂ interface. We pursued detailed calculations to understand the mechanisms that control the preferred atomic arrangements at a Si-SiO₂ interface as a first step in understanding what will happen when radiation effects are considered⁹. We concluded that an abrupt and smooth interface is energetically preferred for two reasons: the topology of the (100) Si surface and the flexibility of the Si-O-Si chain. Nevertheless, there are two energetically degenerate phases at the interface layer that can lead to domain boundaries where suboxide bonds are needed to heal potential dangling bonds. We have constructed several such model interfaces and used them for further calculations of radiation-induced interfacial defects.

Hydrogen reactions with Si-SiO₂ interfaces. We theoretically investigated the reactions of hydrogen atoms and ions (protons) with Si-SiO₂ interfaces^{10,11}. We used density functional theory and supercells confining (100) Si-SiO₂ interfaces which a) are totally abrupt and smooth; b) have SiO₂ protrusions into Si; and c) have suboxide bonds (Si-Si bonds on the oxide side), with all atoms being properly coordinated (2 for O, 4 for Si). We found the following: Both H and H⁺ have a relatively shallow barrier against passing through abrupt interfaces and interfaces with SiO₂ protrusions with minimal interactions, at least in the absence of dangling bonds with which they might otherwise react. Suboxide bonds, however, trap H⁺ in relatively deep wells with an asymmetric barrier: the barrier is relatively small (~1 eV) for H⁺ to exit on the oxide side, but the barrier is much higher (~1.5 eV) for H⁺ to exit on the Si side. In addition, this defect does not have a localized energy level in the vicinity of the Si band gap and thus cannot be neutralized by electrons. Similarly, a neutral H atom can also be trapped in a suboxide bond, but it has an electron at a level that is higher than the conduction band edge of Si. The center loses that electron to the Si side and is then completely equivalent to a trapped H⁺. These results allowed us to account for the proton trapping and cycling behavior that is observed in a unified way.

Proton-induced defect generation at the Si-SiO₂ interface. We showed that H⁺ is the only stable charge state of H at the Si-SiO₂ interface. The protons can diffuse easily in the interfacial plane and remove hydrogen atoms passivating the dangling bonds directly, forming H₂,



Hydrogen molecules are free to leave the interface and leave behind positively charged dangling bonds (D⁺), whose charge state is afterwards controlled by the Si surface potential. Therefore, depassivation of Si-H bonds at the Si-SiO₂ interface occurs as a result of a direct

⁹ R. Buczko, S. J. Pennycook and S. T. Pantelides, Phys. Rev. Lett., vol. 84, pp. 943 – 946, 2000.

¹⁰ S. T. Pantelides, S. N. Rashkeev, R. Buczko, et al., IEEE Trans. Nucl. Sci., vol. 47, pp. 2262 – 2268, 2000.

¹¹ S. N. Rashkeev, D. M. Fleetwood, R. D. Schrimpf, et al., Appl. Phys. Lett., vol. 81, pp. 1839 – 1841, 2002.

reaction with protons. The process is independent of the electron concentration in the substrate^{12,13}.

We find that H^+ at the Si-SiO₂ interface cannot be neutralized by electrons that may tunnel from the Si side (as is widely believed), i.e., that H^+ is the only stable charge state at intrinsic Si-SiO₂ interfaces. Our calculations show that the Si-H bond is highly polar – the electronic density is higher near the H atom than near the Si atom. The total number of electrons in the electronic cloud around the hydrogen atom is about 1.6, i.e., we can say that the H atom shows a high degree of electronegativity. At a distance of approximately 1.6 Å a mutual attraction between the originally "bare" proton (the region surrounding H^+ contains less than 0.3 electrons) and the H atom from the polar Si-H bond was sensed. Then the electronic cloud takes an elongated shape and starts to surround the H^+ ion as well (the total number of electrons around H and H^+ is about 1.85). At last, one observes a creation of a neutral hydrogen molecule and a positively charged D^+ defect at Si.

The role of O₂ and H₂O molecules in irradiated SiO₂ We found that the energetically most favorable configuration of O₂ and H₂O in amorphous silica is an interstitial molecule^{14,15}. The only possible reaction between a water molecule and a perfect amorphous structure is the formation of two silanol groups with a 1.5 eV activation barrier. An oxygen molecule is unlikely to break up: two peroxy radicals would form only at a cost of 0.92 eV with a relatively high (~2 eV) barrier.

The diffusion barrier for water is sensitive to the size of the void it is diffusing in. The various crystalline forms of SiO₂ have six-member rings with typical void size of ~6 Å, whereas in an amorphous network one expects a distribution of void sizes. For the mean ring size of ~6 Å, the calculated diffusion barrier for water is 0.8-0.9 eV and is very certain (just slightly changing from ring to ring). For smaller rings, the barrier increases, up to 2.2 eV for 4-Å rings. For oxygen the situation is different – the barrier can fluctuate between 0.6 eV and 1.0 eV for different 6 Å voids.

From the difference in total energies of interstitial O₂ and H₂O and various possible reaction products with an E' center we found that an annihilation reaction proceeds immediately with a high (>1.9 eV) energy gain. The reaction of an O₂ with a vacancy results in peroxy bond formation and an energy release of 5.45 eV. For O₂ the reaction is barrierless while the annihilation reaction with H₂O has a barrier of 1.3 eV.

E' centers can be generated by γ irradiation in two different ways. First, preexisting oxygen vacancies (E' precursors) may simply capture a hole and become E' centers. The presence of the reaction barrier for annihilation of an E' center by an H₂O molecule, however, results in different annealing rates in [OH]-rich and low-OH] oxides: E' centers are annealed out faster in dry oxides because the O₂ annihilation process is barrierless.

¹² S. N. Rashkeev, D. M. Fleetwood, R. D. Schrimpf, et al., Phys. Rev. Lett., vol. 87, no. 16, 165506, 2001.

¹³ S. N. Rashkeev, D. M. Fleetwood, R. D. Schrimpf, et al., IEEE Trans. Nucl. Sci., vol. 48, pp. 2086 – 2092, 2001.

¹⁴ T. Bakos, S. N. Rashkeev and S. T. Pantelides, Phys. Rev. Lett., vol. 88, no. 5, 055508, 2002.

¹⁵ T. Bakos, S. N. Rashkeev and S. T. Pantelides, Phys. Rev. B, vol. 69, no. 19, 195206, 2004.

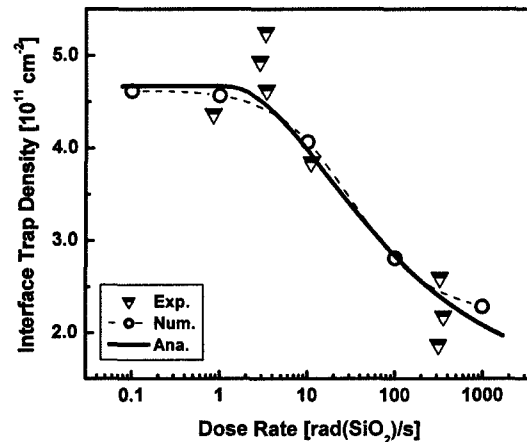


Figure 3.3.1: Experimental, analytical and simulated interface trap density as a function of dose rate for an Analog Devices' RF25 capacitor irradiated to a total dose of 200 krad(SiO₂).

Physical model for enhanced interface-trap formation at low dose rates. The radiation-induced gain degradation of many types of bipolar transistors (BJTs) is greater at low dose rates than at high rates. This enhanced low-dose-rate sensitivity (ELDRS) is an important problem for space systems.

We used rate equations for electrons, holes, and protons plus Poisson's equation to describe the ELDRS phenomenon¹⁶. Interface-trap formation (related to proton reactions at the Si-SiO₂ interface) at high dose rates is reduced due to hole-related positive charge buildup in the Si-SiO₂ interfacial region. The mobility of holes is much higher than the mobility of protons, and the trapped holes can form an electrostatic barrier that prevents the protons from reaching the interface and generating interface traps. At low dose rates, the charge buildup process is reduced, relative to charge transport processes, and both holes and protons can reach the interface and participate in oxide- and interface-trap formation. Our analytical and numerical calculations are in reasonable agreement with available experimental data (Figure). They also explain the dependence of the positive charge buildup on the mobility of the carriers and on the external electric field.

Radiation-induced acceptor deactivation in bipolar devices: Effects of electric field. The radiation-induced gain degradation of bipolar junction transistors (BJTs) is an important problem for space systems. The degradation of BJTs is sensitive to a variety of phenomena, such as dose rate, irradiation temperature, and measurement bias. We used an approach based on analytical modeling and Monte Carlo simulations to focus on the problem of dopant deactivation in p-Si, which forms the base region of NPN BJTs^{17,18}. We found that the dramatic dependence of acceptor neutralization on irradiation bias can be explained, primarily by the direct neutralization of boron by protons in the reaction, $B^- + H^+ \rightarrow (BH)^0$,

¹⁶ S. N. Rashkeev, C. R. Cirba, D. M. Fleetwood, et al., IEEE Trans. Nucl. Sci., vol. 49, pp. 2650 – 2655, 2002.

¹⁷ S. N. Rashkeev, D. M. Fleetwood, R. D. Schrimpf, et al., IEEE Trans. Nucl. Sci., vol. 50, pp. 1896 – 1900, 2003.

¹⁸ S. N. Rashkeev, D. M. Fleetwood, R. D. Schrimpf, et al., Appl. Phys. Lett., vol. 83, pp. 4646 – 4648, 2003.

i.e., one does not need to consider (at least to first order) processes involving neutral hydrogen in the inversion regime. The electric field dependence of the neutralized dopant concentration is defined by the proton transport in the depletion region and can be explained by interplay between the proton diffusion and drift processes (Figure 3.3.2). When the electric field is negative, most of the protons injected into the Si return back to the interface. When the voltage is positive, the protons deposited at the Si-SiO₂ interface move deeper in the Si layer, and the trajectories become longer. The curve has a maximum at small positive bias when the diffusive motion dominates. In this regime, the acceptor passivation rate is maximal.

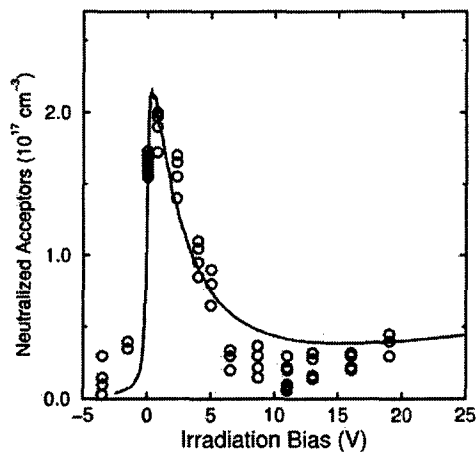


Figure 3.3.2: The concentration of neutralized acceptors as a function of irradiation bias voltage in a p-doped Si layer (solid line) compared with experiment (open circles).

Effects of hydrogen motion on interface trap formation and annealing. We found that the interface-trap formation is totally controlled by the competing processes of depassivation of the hydrogen-passivated interfacial defects by protons and passivation of these defects by neutral hydrogen (presumably, hydrogen molecules)¹⁹. The interplay between these two processes explains the experimentally observed drastic change of the interface-trap formation dynamics that can occur at about 150 °C (Figure 3.3.3).

¹⁹ S. N. Rashkeev, D. M. Fleetwood, R. D. Schrimpf, et al., IEEE Trans. Nucl. Sci., vol. 51, pp. 3158 – 3165, 2004.

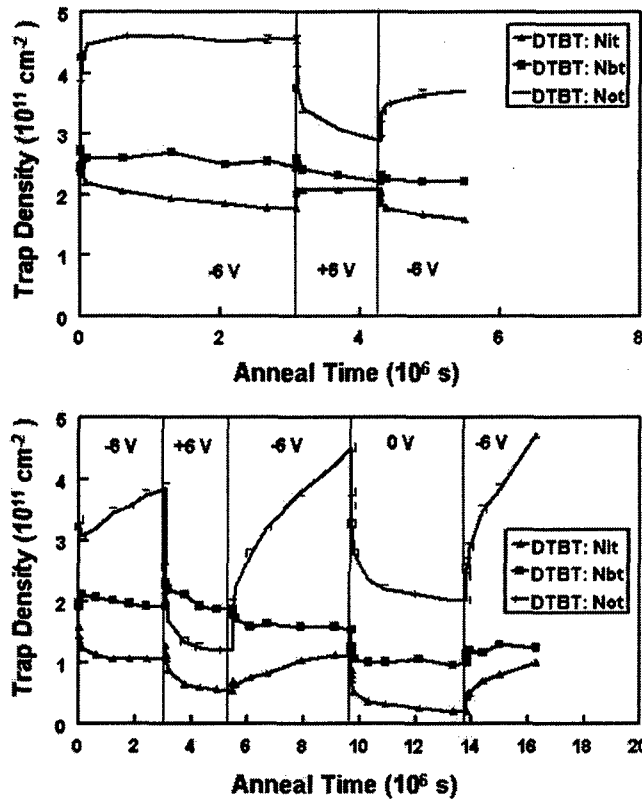
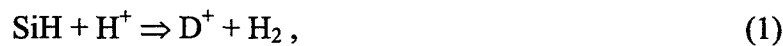


Figure 3.3.3: ΔN_{it} , ΔN_{bt} , and ΔN_{ot} estimated from the "dual-transistor border-trap" (DTBT) technique for annealing temperatures of 80 °C (upper panel) and 150 °C (lower panel). These devices were irradiated to 45 krad(SiO_2) at 6 V with 10-keV x rays at a dose rate of 240 rad(SiO_2), prior to annealing. [After D. M. Fleetwood et al., IEEE Trans. Nucl. Sci., 44, 1698 (1995)].

When the voltage is positive (+6 V), numerical simulations show that N_{it} increases at $T = 80$ °C and decreases at $T = 150$ °C (Figure 3.3.), in agreement with Figure 3.3.3. One reason this occurs is because the depassivation by protons arriving to the interface from the oxide via the reaction:



depends only on the total number of protons that pass through the interface (we always assume that interface traps are mainly related to dangling-bond defects, D; the charge state of these defects is controlled by the potential at the interface, and at positive bias they may be neutral or negatively charged). The depassivation process does not depend on temperature or on the time interval during which the positive bias is applied.

The passivation process



depends not only on the temperature (this dependence is strong because the reaction barrier for passivation is high, ~ 1.5 eV) but also is proportional to the time interval during which the positive bias is applied. As a result, the passivation may start to dominate.

We found that in addition to these processes, storage of neutral molecular hydrogen in Si should occur at positive bias. The protons that do not react at the interface, but go into the Si, likely will be transformed to H^- (hydrogen in Si exhibits so-called “negative U” properties and is unlikely to be neutral once equilibrium is achieved). The transformed negatively charged hydrogen ions (H^-) will move back toward the interface from the Si side and will react with protons at the interface and in the bulk Si,



When the bias switches to negative, the protons in the oxide that did not go into the Si yet (when the bias was positive) and did not react will drift away from the interface. This means that the flux of protons across the interface is weak or absent until some new source of protons is turned on. Therefore, at lower temperatures, the interface-trap annealing by the H_2 molecules at the interface dominates over the depassivation of dangling bonds (see the curve in Fig. 3.3.4 for 80°C). The proton flux from the Si will increase when immobile H_2 molecules that have been formed in the process (equation 3) and stored in the bulk Si start to dissociate. At higher temperatures, the flux of protons arriving at the interface from the Si increases. As a result, N_{it} grows initially much more rapidly at 150°C than at room temperature.

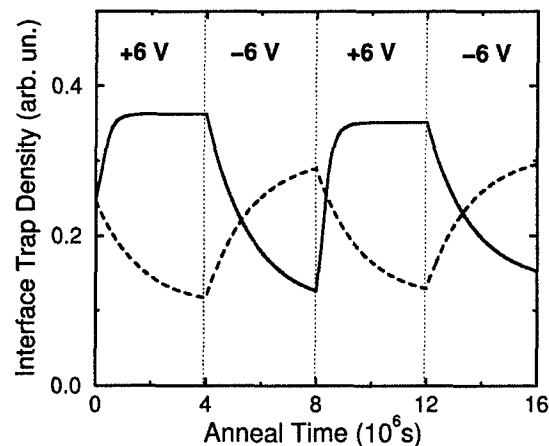


Figure 3.3.4: Interface-trap density as a function of time, temperature, and bias voltage. The solid line corresponds to $T = 80^\circ\text{C}$, the dashed line to $T = 150^\circ\text{C}$.

An important conclusion here is that both buildup and annealing of interface traps are controlled by the mobility and trapping of different hydrogen species near the Si-SiO₂ interface.

3.4 Contactless Characterization of Radiation-Induced Defects Using Intense, Tunable, Ultra-fast Laser Techniques

Second-Harmonic Generation (SHG) has proven to be a sensitive probe of buried interfaces and may become a very useful tool in monitoring the quality semiconductor devices. We have developed a contactless two-color optical technique that allows us to monitor carrier transport (injection, tunneling) by multiphoton internal-photoemission induced second-harmonic generation. Using our technique we were able to measure the Si/SiO₂ band-offset. One- and two-photon internal-photoemission thresholds were measured to be 4.5 eV and 2.25 eV respectively. We have also used this technique to measure X-ray irradiation enhanced electron transport across thin-oxide Si/SiO₂ samples. Measured electron transport rates across an irradiated oxide were found to be substantially higher in comparison to unirradiated oxides. This effect is attributed to the presence of X-ray irradiation induced defects that act as intermediate trapping sites facilitating enhanced electron tunneling through the oxide. In addition, we have shown for the first time that optical SHG measurements can be performed effectively on an oxide sample with a gradually varying thickness (from 1 nm to 6.5 nm). The significant differences in carrier-dynamics behavior in thin (~ 1 nm) and thick (~ 6 nm) oxide layers on the same sample using SHG give unique insight into conventional electron tunneling processes as well as radiation-induced transport mechanisms in thin oxide films. These results are particularly important since conventional electrical measurements used in radiation effect studies cannot be performed effectively on an oxide sample with gradually varying thickness ultrathin oxides. Because of the demonstrated importance of this new approach, we have designated it as Laser Interrogated Leakage Current (LILC).

We also have demonstrated that SHG can be used to monitor interface quality and charge carrier dynamics in across Si/SiO₂/Si (SOI) interfaces. SHG signal from SOI wafers depends strongly on the externally applied electric field. This can be explained by the different contributions of each of the SOI interfaces. The differences observed when external electric fields were applied may be attributed to the difference in quality between top and the bottom interfaces. Electrical and optical measurements have also been compared showing strong correlation between *I-V* characteristic and the EFISH technique.

For centro-symmetric materials such as crystalline Si, second order nonlinear susceptibility vanishes. However at the interface the symmetry is broken and optical nonlinear processes are allowed. This gives one a unique opportunity to study properties of buried interfaces. In particular, Si/SiO₂ interfaces have been studied extensively, and significant progress has been made in understanding the sensitivity of the second-harmonic generation to interface defects, stress, strain, roughness, and chemical modification of interfaces. In addition, the SHG signal is sensitive to the electric field at the interfaces. Electric field induced second-harmonic (EFISH) response can arise due to intrinsic fields, externally applied fields and/or the result of separation of photo-induced charges. That allows us to effectively study carrier dynamics at semiconductor interfaces.

Our results on Si/SiO₂ show that wavelength-dependent two-color SHG measurements can provide information about basic properties of the interface, such as carrier injection thresholds, which are related to the band offset. We have made first measurements of the Si valence to SiO₂ conduction band offset via multiphoton internal-photoemission induced second-harmonic generation. The number of photons required to inject electrons from silicon

to SiO₂ was determined for several different energies in a range of pump photon energies (1.9-4.8 eV) (Figure 3.4.1). We observe the stepwise jumps from one- to two-photon (between 4.56 and 4.50 eV) and then from two- to three-photon (between 2.30 and 2.20 eV) processes, as the incident pump energy decreases. The energies for stepwise jumps are identified as the thresholds for one-photon (~ 4.53 eV) and two-photon (~ 2.25 eV) electron injection from Si valence band into SiO₂ conduction band. To the best of our knowledge, this is the first time that multiphoton internal photoemission thresholds were observed.

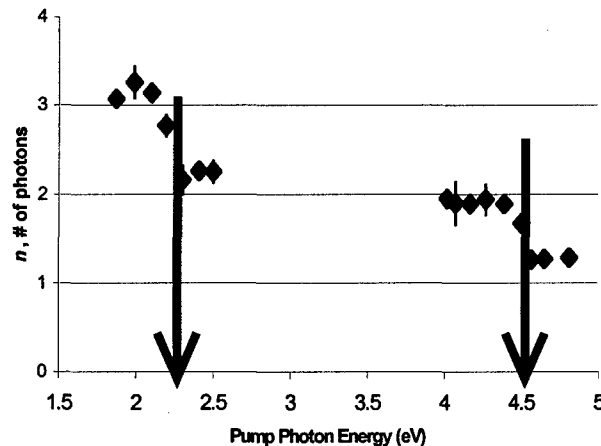


Figure 3.4.1: The order of electron injection process from Si into SiO₂ versus pump photon energy.

We have showed that multiphoton internal-photoemission induced second-harmonic generation promises to become a valuable experimental tool in determining band offsets in a wide variety of semiconductor interfaces including many new alternate and chemically modified oxides under investigation. This novel contactless technique can be easily applied for most systems where the two materials in contact are isotropic or amorphous.

Carrier movement (injection, transport, tunneling, and recombination) and charge trapping in gate oxides are essential factors in understanding semiconductor device performance and degradation, especially in a radiation environment. In addition to the population of precursor defects with trapped charge and the possible generation of new traps, X-ray irradiation also may influence the carrier dynamics at interfaces. It has been shown recently that high doses of ionizing radiation in thin oxides (40-60 Å) may cause Radiation Induced Leakage Current (RILC). The conduction mechanism in RILC (as well as in Stress Induced Leakage Current, SILC) has been attributed to neutral oxide defects, which mediate electron tunneling across the oxide. Presently, characterization of radiation damage in Si/SiO₂ systems is usually accomplished with electrical methods such as capacitance-voltage (C-V) and current-voltage (I-V) measurements. We use a novel two-color technique, based on time-dependent electric field induced SHG, for direct measurements of changes in electron transport characteristics due to X-ray irradiation in thin oxides to characterize the radiation response of a SiO₂ film on Si(100). We find that the detrapping rate of surface charge in the X-ray irradiated devices is much higher than that of unirradiated devices.

In addition we applied our optical technique to measure electron transport in a variable-thickness ultra-thin SiO₂-on-Si structure (1.0-6.5 nm). In our experiment, we used samples with a Si (100) substrate and an initial SiO₂ oxide thickness of 6.5 nm. The sample was dipped into a 1% solution of hydrofluoric acid at a controlled speed to provide a gradually decreasing thickness of the oxide film.

One half of the variable thickness Si/SiO₂ sample was irradiated to a 20 Mrad total dose by 10 keV X-ray source at a dose rate of ~1 krad(SiO₂)/s. The masked side of the film was not irradiated, and served as a control to help understand the effects of irradiation on charge transport in ultra-thin film SiO₂. These experiments showed for the first time that optical SHG measurements can be performed effectively on an oxide sample with a gradually varying thickness (from approximately 1 nm to 6.5 nm). The significant differences in carrier-dynamics behavior in thin (~ 1 nm) and thick (~ 6 nm) oxide layers on the same sample using SHG give unique insight into conventional electron tunneling processes as well as radiation-induced transport mechanisms in thin oxide films (Figures 3.4.2 and 3.4.3).

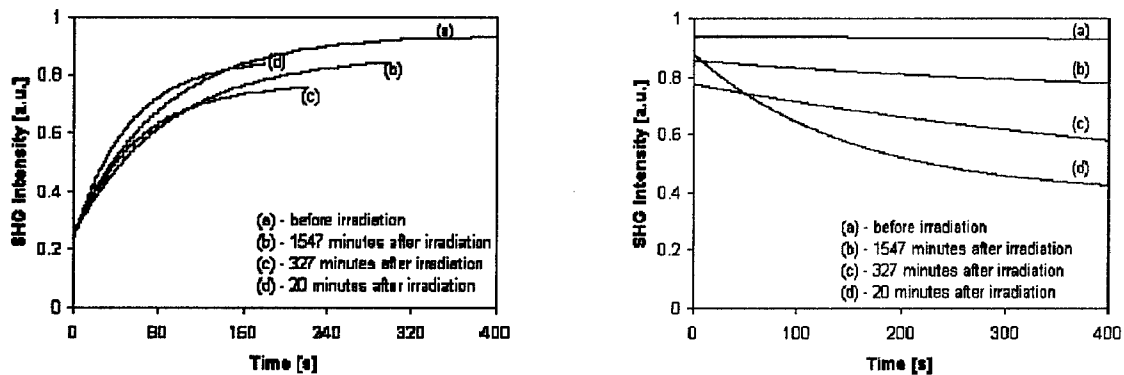


Figure 3.4.2: Exponential fits of time-dependent SHG signals from the thick part of the oxide layer (left – injection; right – recombination).

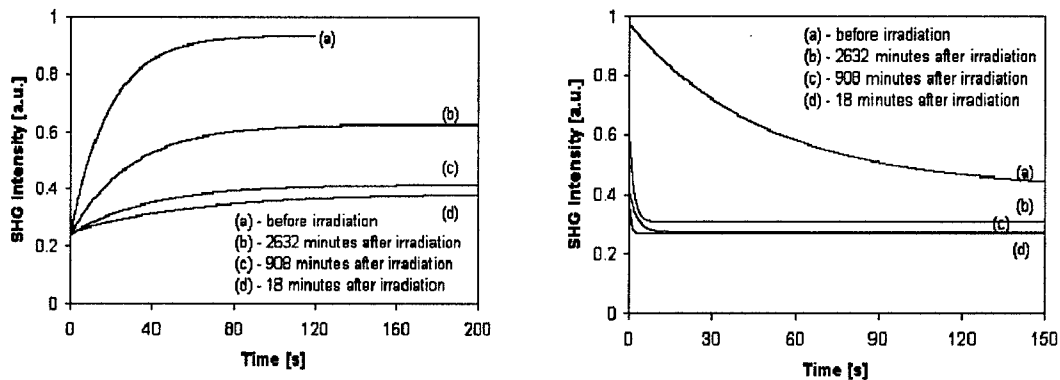


Figure 3.4.3: Exponential fits of time-dependent SHG signals from the thin part of the oxide layer (left – injection; right – recombination).

Since our oxides have no gate electrode we cannot detect electrical leakage directly. Instead we measure time-dependent changes in the electric field across the oxide associated with charge transport and trapping via LILC. We emphasize that this method is capable of observing X-ray irradiation induced leakage at much lower doses than those at which one is typically able to detect radiation induced leakage current (RILC) in SiO_2 films via electrical measurement techniques. This is indicative of the relative large sensitivity of this technique. The defects associated with LILC are observed to anneal at room temperature, while RILC/SILC mediating defects anneal only at elevated temperatures. It is probable that the LILC technique characterizes processes that are precursors to electrically detectable RILC in SiO_2 .

Our experimental technique is also proven to be a sensitive probe of electric field at silicon on insulator (SOI) interfaces and allows us to monitor charge transfer across $\text{Si}/\text{SiO}_2/\text{Si}$ interfaces. The time-dependent SHG signals showed a strong dependence on an externally applied electric field. The internal electric fields at the two interfaces are believed to be responsible for the asymmetry shown in Figure 3.4.4. Electrically induced carriers are responsible for the asymmetric behavior in channel current (inset figure in Figure 3.4.4). The optical measurements exhibited a similar trend, implying that the noninvasive optical technique can be used for material property characterization.

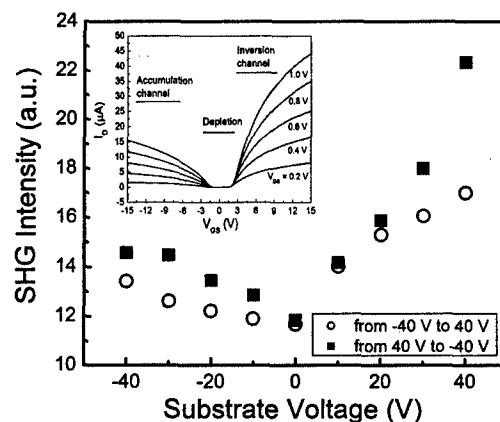


Figure 3.4.4: Time-dependent SHG signal from a Si film with applied DC bias across the BOX. The inset figure shows electrical characteristics from direct probing.

In summary, we have shown that noninvasive and contactless second-harmonic generation can be used to monitor important properties of semiconductor/insulator systems. We have made first measurements of the Si valence to SiO_2 conduction band offset via multiphoton internal-photoemission induced second-harmonic generation. We have showed that multiphoton internal-photoemission induced second-harmonic generation promises to become a valuable experimental tool in determining band offsets in wide variety of semiconductor interfaces including many new alternate and chemically modified oxides under investigation. We determined that the electron-tunneling rate decreases with time at room temperature after X-ray irradiation, indicating that the electron transport-mediating traps may be annealed at room temperature. This is in contrast with annealing studies

performed at substantially higher temperatures on RILC, suggesting that the defects responsible for the Laser Interrogated Leakage Current (LILC) observed in our experiments are either (1) defect precursors (observable at lower dosages due to increased sensitivity), or (2) different than, the defects responsible for RILC. It is likely these defects are O vacancies (E' centers) or hydrogen-related. We have applied this technique to investigate properties of multilayer systems, such as SOI with different fabrication histories. We suggest that one may be able to adapt this technique as a method of in situ monitoring of the quality of thin dielectric layers.

3.5 Characterization of Radiation Defects in Microelectronic Structures Using Physical and Electrical Characterization Techniques

3.5.1 Objectives (Ohio State)

At Ohio State University, researchers probed the energies, densities, and spatial distributions of radiation-induced traps in MOSFETs, capacitors, and HEMTs using lateral and depth-resolved cathodoluminescence spectroscopy (CLS), spatially-resolved Secondary Ion Mass Spectrometry (SIMS), and a complement of electrical and electronic characterization probes of device parameters. The design of microelectronic structures with improved resistance to the effects of space radiation involves the control of electrically-active defect states. In turn, such control requires understanding how the properties of such defects depend on the local chemical bonding environment and how ionizing radiation activates these defects. The spatial distribution of sub-band gap luminescence within these materials and their device structures provides information on the microscopic formation and electronic evolution of defects due to irradiation.

In the context of the overall MURI, The Ohio State group's goal was to identify physical mechanisms underlying formation of radiation-induced defects and methods to mitigate such effects via novel materials and processing. To achieve this objective, we have probed energies, densities, and spatial distributions of electronic traps in Si MOSFETs and capacitors, as well as AlGaIn/GaN HEMTs, MODFETs, and Schottky barriers irradiated with x-ray and particle radiation using lateral and depth-resolved electron-excited luminescence spectroscopy. In particular, we have used low energy electron-excited luminescence spectroscopy (LEEN) to assess traps induced in thick gate oxide structures when exposed to X-ray irradiation. Using this technique, we extended our radiation-induced defect studies to correlate the electronic performance of AlGaIn/GaN HEMTs and GaN Schottky barriers with deep trap levels over a wide range of irradiation fluences.

3.5.2 Final Status of the Effort (Ohio State)

The Ohio State University group used low energy electron-excited luminescence spectroscopy (LEEN) and high energy micro-cathodoluminescence spectroscopy (CLS) to probe the electronic properties of Si MOSFETs and capacitors, AlGaIn/GaN HEMTs, MODFETs, and Schottky barriers and the effects of x-ray or proton irradiation. These studies provide maps of the positions of radiation induced trap centers within the semiconductor structures, either laterally or in depth on a nanometer scale. Such measurements can thereby reveal the physical mechanisms underlying

changes in electronic properties of advanced semiconductor device structures with x-ray or particle radiation.

Depth-resolved LEEN spectra of ultrathin SiO₂/Si interfaces irradiated with 10 keV X-rays reveal that multiple 7.6 Mrad doses produce defect emissions localized within or near the 5 nm oxide. Emissions corresponding to E' oxygen vacancies (positively charged oxygen vacancy in SiO₂) are evident near the SiO₂/Si interface after 15 Mrad doses. Further increases in this emission due to time-dependent effects are apparent. Emissions corresponding to non-bridging oxygen hole centers (NBOHC) in SiO₂ are also present.

In terms of state-of-the-art advances, these results represent the first documented observations of optical emission due to X-ray irradiation. The measurements yield characteristic spectral energies of known oxide defects (1.9 eV NBOHC) and 2.7 eV E'), the measurements have nanometer-scale depth resolution, X-ray doses of 5 nm-thick oxide films induce $\sim 5 \times 10^{11} \text{ cm}^{-2} \text{ eV}^{-1}$ with optical threshold detection density of $\sim 10^{11} \text{ cm}^{-2} \text{ eV}^{-1}$, and the excitation depth dependence enable us to separate the spatial variations of the E' versus NBOHC defects near the Si/SiO₂ interface. Overall, these results show relatively small changes in trap features, demonstrating that ultra-thin dimensions of gate oxides minimize creation of new traps by X-rays.

Cross sectional CLS spectra of Si/1.05 micron SiO₂/Al capacitors irradiated with 10 keV X-rays (0.58 krad (SiO₂) dose) show that irradiation increases E' emission at the Al-SiO₂ interface while it decreases E' defect density at the Si-SiO₂ interface. Ultrahigh vacuum micro-potential measurements from secondary electron thresholds display clear variations in work function across the 1- μm dielectric, increasing monotonically by 1.7 eV from the Al/SiO₂ gate interface to the Si/SiO₂ interface.

In terms of state-of-the-art advances, these cross sectional CLS and work function measurements provide the first observations of optical emission from traps induced by X-ray irradiation in devices. The measurements yield characteristic spectral energies of known oxide defects, the measurements have a spatial resolution of 50-100 nm within the oxide, and cross sectional dependence identifies relative variations of trap densities from gate to channel. Overall, these results are consistent with E' precursor (neutral oxygen vacancy) defects trapping radiation -generated holes.

AlGaN/GaN high power, high frequency transistors are strong candidates for key aerospace and satellite applications and radiation effects represent an important consideration. While GaN exhibits a hundred-fold improvement in radiation hardness versus GaAs, nevertheless relatively little is known about the nature of III-N radiation damage, e.g., defects, field distributions, radiation effects on the piezoelectric field-induced channel structure is not yet understood, and device structures are difficult to characterize electrically or optically because of their ultrathin film dimensions. We used depth-resolved LEEN spectroscopy to probe radiation effects in modulation doped field effect transistors (MODFETs) grown by our UCSB team members and irradiated with 1.8 MeV proton by our Vanderbilt team members. These studies reveal a decrease in ~ 3.8 eV emissions due to electrical field decreases in the AlGaN layers,

an increase in 2.25 eV emission due to Ga vacancy-related complexes near the AlGa_N surface, and an increase in 3.8 eV emissions due to higher electric fields near the AlGa_N outer interface. Analogous measurements at AlGa_N/Ga_N high electron mobility field effect transistors (HFETs) also show a decrease in electrical field within the AlGa_N layers but show a significantly stronger effect on existing bound states, i.e., a new defect peak at ~3.19 eV along with decreases in the 3.42 eV donor bound exciton and 3.2-3.4 eV stacking fault defect emissions. 1.8 MeV proton doses show strong decreases of AlGa_N/Ga_N transistor saturation current and increases in threshold voltage above 10^{13} p⁺/cm², with transconductance degrading rapidly above 10^{14} p⁺/cm². Transfer length measurements of these transistors display sublinear increases in contact resistivity through 10^{14} p⁺/cm² and significant degradation above 10^{14} p⁺/cm². Hall effect measurements reveal that mobility degrades at lower proton doses before 2-dimensional electron gas (2DEG) sheet density. AlGa_N/Ga_N SIMS interface profiles of these irradiated AlGa_N/Ga_N interfaces reveals a broadening with increasing fluence of at least 2.5 nm at 10^{15} p⁺/cm². These results can be interpreted as acceptor states due to Ga vacancy complexes compensating the Si doping in the AlGa_N layer and decreasing the charge in the 2DEG channel, lowering the Fermi level in the Ga_N. Detailed studies of transistor threshold voltage, contact resistivity, Schottky barrier, channel density and mobility versus proton fluence beyond 2×10^{15} p⁺/cm² reveals significant mobility degradation above 10^{14} p⁺/cm² that accounts for transconductance and saturation drain current changes. These correlate with CLS and SIMS results that indicate AlGa_N/Ga_N interface roughening. Above 2×10^{15} p⁺/cm², significant 2DEG charge density occurs, indicating that the polarization charge must dominate the threshold voltage. This is consistent with CLS spectra that indicate AlGa_N/Ga_N intermixing and electric field lowering.

In terms of state-of-the-art advances, these results represent the first direct optical observation of proton-induced degradation mechanisms inside AlGa_N/Ga_N 2DEG transistors. These involve: Ga_N compensation of existing donors (significant at $\geq 10^{13}$ p⁺/cm²), 2DEG channel mobility decreases (dominant at $>3 \times 10^{14}$ p⁺/cm²), and 2DEG carrier density decreases (dominant in the 10^{15} p⁺/cm² range). Our results also identify defects created by proton damage (Ga vacancies and/or complexes) and their dose dependence. Finally, these results resolve the physical basis for AlGa_N/Ga_N transistor degradation – Fermi level lowering and interface roughening as opposed to lattice relaxation. Perhaps most significant is that major degradation of transistor transconductance, threshold voltage, mobility, contact resistivity and Schottky barrier take place but only at doses of 10^{14} - 10^{15} p⁺/cm², indicating the superior radiation hardness of this device material.

We also investigated radiation effects of 1.8 MeV protons on Ga_N-metal Schottky barriers. These studies revealed Schottky barrier lowering of 5% at high doses of 10^{14} p⁺/cm². Associated with this effect, series resistance increases and effective doping decreases linearly through 3×10^{13} p⁺/cm², extrapolating to an insulating transition at 10^{14} cm⁻² dose. Irradiation with 1.0 MeV decreases doping (Schottky barrier) 1.7 x (2 x) faster, corresponding to a maximum vacancy density of 8×10^{16} cm⁻³ from 10^{13} p⁺/cm² as calculated using TRIM. Indeed the differences in effective doping decreases between 1.8 and 1.0 MeV proton irradiation follow the vacancy production ratio.

Annealing at relatively low (200 °C) temperatures recovers most of these decreases. Micro-CL spectra of these irradiated GaN show that the dominant near-surface radiation effect is increased “yellow luminescence” commonly attributed to Ga vacancies and vacancy complexes.

In terms of state-of-the-art advances, these irradiated Schottky diode studies provide a direct correlation of proton-induced defects at GaN diodes with Schottky barrier and effective doping changes. The Schottky barriers and effective doping both decrease with p^+ fluence. MeV protons decrease Schottky barriers for relatively low ($\sim 10^{11}/\text{cm}^2$) doses. These irradiation-induced changes in Schottky barrier and doping are consistent with TRIM calculations of defect production. Their effects can be mitigated by moderate temperature annealing. The defects created by proton damage and their dose dependence have been identified and shown to be deep acceptors that compensate carrier concentration.

3.5.3 Accomplishments/New Findings

- The first documented observations of optical emission due to X-ray irradiation. The low ($\sim 5 \times 10^{11} \text{ cm}^{-2} \text{ eV}^{-1}$) defect concentrations induced in ultrathin oxide films by large (10 keV X-rays, multiple 7.6 Mrad (SiO_2)) doses demonstrates that ultra-thin dimensions of gate oxides minimize creation of new traps by X-rays.
- The first observations of optical emission from traps induced by X-ray irradiation in devices. Measurements for Si/ SiO_2 /Al capacitors are consistent with E' precursor (neutral oxygen vacancy) defects trapping radiation –generated holes.
- The first direct optical observation of proton-induced degradation mechanisms inside AlGaIn/GaN 2DEG transistors. Key mechanisms are: GaN compensation of existing donors (significant at $\geq 10^{13} \text{ p}^+/\text{cm}^2$), 2DEG channel mobility decreases (dominant at $> 3 \times 10^{14} \text{ p}^+/\text{cm}^2$), and 2DEG carrier density decreases (dominant in the $10^{15} \text{ p}^+/\text{cm}^2$ range). Our results also identify defects created by proton damage (Ga vacancies and/or complexes) and their dose dependence. These results resolve the physical basis for AlGaIn/GaN transistor degradation – Fermi level lowering and interface roughening as opposed to lattice relaxation. Significantly, major degradation of transistor and barrier properties take place only at doses of 10^{14} - $10^{15} \text{ p}^+/\text{cm}^2$, indicating the superior radiation hardness of this device material.
- Direct correlation of proton-induced defects at GaN diodes with Schottky barrier and effective doping changes. These effects can be mitigated by moderate temperature annealing. The defects created by proton damage (Ga vacancies and their complexes) and their dose dependence have been identified and shown to be deep acceptors that compensate carrier concentration.

Overall, we have reached our project objectives: We have identified physical mechanisms underlying formation of radiation-induced defects and methods to mitigate these effects via novel materials and processing. Two such candidates are (1) ultrathin film dielectrics that present a low volume for damage and (2) radiation-hard AlGaIn

and GaN. We have probed the energies, densities, and spatial distributions of electronic traps in leading device structures, including Si MOSFETs metal-SiO₂/Si capacitors, AlGaIn/GaN MODFETs, HFETs, and Schottky barriers, irradiated with x-ray and particle radiation using lateral and depth-resolved electron-excited luminescence spectroscopy.

3.6 Proton Irradiation Effects on III – V Compound Semiconductor Devices

This research effort was aimed at gaining a better understanding of the effects of particle radiation on compound semiconductor (III – V) devices. Compound semiconductor devices have emerged as promising candidates for space-borne applications because of their high-power, high-frequency capabilities. Moreover, it is necessary to qualify these devices for the space radiation environment in order to employ them on board space-based systems. At Vanderbilt University, both gallium arsenide and gallium nitride based devices were studied for their radiation response. These devices were fabricated at the University of California, Santa Barbara (UCSB). Metalorganic chemical vapor deposition (MOCVD) process was used to deposit the devices. The devices were diced and packaged at the Air Force Research Laboratory (AFRL).

AlGaAs/GaAs heterojunction bipolar transistors (HBTs) were irradiated with 1.8 and 105 MeV protons. The device degradation was observed as increase in the base current and decrease in the collector current, leading to gain degradation after irradiation. The increase in base current was observed to be the result of displacement damage induced traps that led to decreased minority carrier lifetimes. The decrease in collector current was due to the deterioration of emitter – base diode that led to decreased electron injection efficiency²⁰.

Proton irradiation studies were also carried out on GaN-based high electron mobility transistors (HEMTs). AlGaIn/GaN HEMTs were exposed to 1.8, 15, 40 and 105-MeV protons. It was observed that lower energy protons caused significantly higher damage than higher energy protons²¹. AlGaIn/AlN/GaN HEMTs and GaN/AlGaIn/GaN HEMTs were irradiated with 1.8-MeV protons to assess their radiation tolerance^{22,23}. AlGaIn/AlN/GaN HEMTs and GaN/AlGaIn/GaN HEMTs continued to operate normally up to a fluence of $\sim 10^{14}$ cm⁻². The devices showed significant deterioration in electrical characteristics after this fluence level. The device degradation was observed through the change in the device threshold voltage, decrease in the drain saturation current and decrease in the device transconductance after irradiation. From the electrical characteristics of the HEMTs, it was observed that radiation induced degradation in sheet carrier density and mobility, increase in the resistance of the thin film structure and changes in the barrier height at the Schottky gate are primarily responsible for device deterioration.

The energy transferred by incident protons to atomic recoils, i.e., the non-ionizing energy loss (NIEL), in the crystal lattice leads to atomic displacements. The energy absorbed by gallium atoms is primarily responsible for atomic displacements that create charged defect

²⁰ X. Hu, B. K. Choi, H. J. Barnaby, et al., IEEE Trans. Nucl. Sci., vol. 49, pp. 3213 – 3216, 2002.

²¹ X. Hu, B. K. Choi, H. J. Barnaby, et al., IEEE Trans. Nucl. Sci., vol. 51, pp. 293 – 297, 2004.

²² X. Hu, A. P. Karmarkar, B. Jun, et al., IEEE Trans. Nucl. Sci., vol. 50, pp. 1791 – 1796, 2003.

²³ A. P. Karmarkar, B. Jun, D. M. Fleetwood, et al., IEEE Trans. Nucl. Sci., vol. 51, pp. 3801 – 3806, 2004

centers. In case of the HEMTs, the defect centers introduced in the crystal lattice lead to carrier removal through charge compensation. Free carriers in the crystal lattice are captured by the defect centers, resulting in decreased carrier density. Also, the charged defect centers increase carrier scattering in the 2-DEG through Coulomb interactions leading to reduced carrier mobility. Radiation-induced defect centers reduce carrier mobility in the thin film structure and increase the device resistance, whereas a change in Schottky barrier height alters the sheet carrier density, leading to degradation of the device characteristics of the HEMTs.

From the preceding discussion, it can be seen that III-V devices show extremely good radiation tolerance. The radiation induced degradation in III-V devices is primarily due to displacement of atoms from the crystal lattice. Moreover, lower energy particles cause more damage than higher energy particles because of higher NIEL.

3.7 Proton Radiation Effect in Stripe Lasers and Vertical Cavity Surface Emitting Lasers (VCSELs)

3.7.1 Objectives

Dramatic growth in the use of optics for both military and commercial space-based applications has motivated our study of radiation effects on optical and optoelectronic components/systems. Additional motivation for this work derives from the basic science required to understand radiation effects in strongly confined structures such as semiconductor lasers. The University of Arizona has had two primary objectives throughout this component of the MURI activity. Our first goal was to understand the basic physics as well as the device-level implications of proton radiation on both stripe and vertical cavity semiconductor lasers. We pursued extensive modeling and simulation as well as experimental validation in the accomplishment of this goal. Our second goal was to extend our device-level modeling activities to the system level. Toward this goal we have developed a library of optical and optoelectronic component models that can be used to realize OE system studies in the presence of various types of radiation damage.

3.7.2 Status of Effort

All of the proposed MURI activities have been completed; however, the University of Arizona is continuing to pursue research on the system-level implications of radiation effects. The MURI has provided us with important insights concerning the complex interactions among components and their individual damage/failure mechanisms. In addition, we have developed an extensive suite of modeling tools for use in simulation studies of radiation effects on optical and OE systems. At this time we feel well-prepared to pursue optical system-level studies that will contribute to the growing understanding of rad-hard design methodologies.

3.7.3 Accomplishments/New Findings (Program Summary)

Stripe Lasers:

1. We experimentally distinguished two important types of damage: lifetime and threshold damage. This work pioneered the use of electrical measurements for characterization of semiconductor lasers.
2. When corrected for lifetime effects we found that the threshold damage factor shows good correlation with NIEL.
3. We discovered an important annealing effect, demonstrating that optical power can recover via laser operation.
4. We developed powerful static MQW laser models that include the effects of non-radiative recombination, free carriers, optical absorption and refractive index perturbation. These models were found to agree well with measurements.
5. We developed a physical model of laser wavelength damage and verified this model via measurements.

Vertical Cavity Lasers:

1. We confirmed the expected behavior of laser threshold current in the presence of displacement damage: non-radiative recombination increases laser threshold.
2. We discovered that radiation damage will have a deleterious effect on the leakage current in VCSELS, shifting the leakage rollover to lower currents.
3. We developed an extensive model of leakage current degradation and confirmed this model via experiments.
4. Using the same physical mechanisms of carrier removal and mobility degradation required to explain the leakage rollover shift, we were able to predict the refractive index change and the resulting wavelength shift in VCSELS.

OE Systems:

1. We developed modeling and simulation tools that facilitated the study of interactions among numerous optical and OE components. Example components in our radiation effects library include lasers (threshold shift, power degradation, wavelength and leakage shifts, etc.), lenses (photodarkening, index shifts, and induced aberrations), gratings (reduced efficiency and angle perturbations), fibers (increased loss from color centers and modal perturbations from index changes), EDFAs (reduced gain, increased ASE), and various detectors (reduced responsivity and increased dark current).
2. We have extended the time-domain models to include both space- and time-domain perturbations.

3. We have exercised these system-level models to predict performance degradations in grating multiplexers/demultiplexers and WDM fiber communication systems.

3.8 Electronic Structure and Interface Properties of High-k Dielectric Gate Stacks in Advanced Si Devices

This portion of the report summarizes the results relevant to intrinsic limitations to the performance and reliability of gate stacks that include transition metal high-k gate dielectrics.

3.8.1 Interface properties for Si devices

The performance and reliability of aggressively-scaled CMOS field effect transistors that include deposited high-k dielectrics and interfacial SiO₂ interlayer dielectrics are determined in large part by electronically-strain driven chemical bonding effects at these interfaces. This includes self-organizing bonding changes at interfacial transition regions with SiO bonding at Si-SiO₂ interfaces²⁴, and fixed charge reduction through self-organizations at internal SiO₂-high-k dielectric interfaces²⁵.

These are addressed quantitatively by application of bond constraint theory (BCT) by extending a methodology first applied to bulk glass formation in oxides and chalcogenides to oxide interfaces²⁶. The method relies on a linear relationship between the number of bonds per atom, N_{av} , and bond-stretching and bending constraints per atom, C_{av} . In ideal glass formers, e.g., SiO₂, C_{av} is equal to the network dimensionality of 3. When $C_{av} > 3$, strain builds up, breaking bonds, and leading to defect formation. The density of defects, D , scales as $[N_{av} - N_{av}^*]^2$, where $N_{av}^* = 2.4$ corresponds to an ideal glass with $C_{av} = 3$. This scaling has been extended to oxide dielectric interfaces, where D is proportional to the square of the step in N_{av} , ΔN_{av}^2 , across a dielectric interface²⁶.

Bond strain at Si-SiO₂ interfaces is partially relieved through the formation of an interfacial transition region with average sub-oxide bonding. XPS studies indicate a random distribution of Si-O arrangements in thermally and plasma as-grown interfaces. After an anneal at 900°C, the in-plane bonding becomes distinctly non-random with Si and O rich regimes, reducing g of in-plane bond-strain, and elimination of optically active defects as observed by cathodoluminescence spectroscopy (CLS). The scale of self-organization is nano-regime, and with likely nucleation sites being associated with dangling bond formation in the Si substrate at densities in the low to mid 10^{12} cm⁻²/cm₂. This assumption predicts a self-organization scale of about 5 nm, similar to strain-induced chemical phase separation in bulk SiO thin films. Based on a difference of ~0.05 nm between Si and O rich structures, this predicts a roughness parameter of the ~2.5 nm, exactly what has been reported for both p-channel and n-channel FETs²⁷.

Bond-strain at internal dielectric interfaces between SiO₂ and alternative dielectrics scales as $\Delta N_{av}^{1.9}$, across at these interfaces. Defects at internal interfaces between SiO₂

²⁴ G. Lucovsky and J.C. Phillips, *J. Vac. Sci. Technol.*, B 22, 2087 (2004).

²⁵ G. Lucovsky, J.P. Maria and J.C. Phillips, *J. Vac. Sci. Technol.*, B 22, 2097 (2004).

²⁶ G. Lucovsky et al., *J. Vac. Sci. Technol.*, B 18, 1724 (2000).

²⁷ S. Takagi, A. Toriumi, M. Iwase and H. Tanjo, *IEEE Trans. Electron Devices* 41, 2357 (1994).

and Zr and Hf based dielectrics are reduced by annealing to $\sim 800^\circ\text{C}$. Based on the $\text{SiO}_2\text{-HfO}_2$ and ZrO_2 equilibrium phase diagrams, as well as experiments, bulk and interfacial silicate bonding is unstable against a separation into SiO_2 and HfO_2 or ZrO_2 . Application of BCT demonstrates that this separation in which SiO_2 encapsulates Hf(Zr)O_2 nano-crystals prevents in-plane bond-strain percolation reducing defect densities. Most of the proposed high-k transition metal and rare earth silicates and aluminates have stable phases between the end-member oxides, and these block self-organizations, preventing fixed charge reductions. Examples include $\text{Al}_2\text{O}_3\text{-SiO}_2$, $\text{Si}_3\text{N}_4\text{-SiO}_2$, and group IIIB TM and trivalent RE oxides and SiO_2 . In this regard all aluminates are rejected as replacement dielectrics with SiO_2 interlayers, simply because both end-member oxide constituents have N_{av} values greater than that of SiO_2 . This criterion for fixed charge reduction, as well as the necessity for an interlayer SiO_2 dielectric with a self-organized SiO interfacial transition region i) limits the choice of high-k dielectrics to Zr and Hf oxides and silicates, and ii) EOT scaling to ~ 0.8 nm.

3.8.2 Electronic Structure of High-K Dielectrics

Experimental Studies

This portion of the research has focused on the band edge electronic structure of high-k gate dielectrics. These dielectrics are qualitatively different than SiO_2 and Si oxynitride alloy gate dielectrics. The conduction band edge states in the high-k dielectrics are derived from highly localized atomic d-states of transition metal (TM) and trivalent lanthanide rare earth (RE) atoms, whereas the conduction band edge states of SiO_2/Si oxynitride alloy dielectrics are derived from more free-electron extended atomic s-states.

High-resolution spectroscopic studies of transition metal (TM) elemental, and TM/rare earth (RE) complex oxide x-ray absorption spectra (XAS) have demonstrates multiple d-state features associated with Jahn-Teller symmetry reductions. As noted above, electron states at the conduction band edge of SiO_2 are derived primarily from Si $3s^*$ states mixed with O $2p^*$ states and are free-electron-like²⁸, whereas band edge states in high-k dielectrics are derived from TM/RE d^* -states mixed with O $2p^*$ states and are considerably more localized²⁹. Jahn-Teller term splittings involving localized d^* -states have been studied by combining x-ray and UV spectroscopy with published results for photoconductivity (PC) and internal photoemission (IPE)³⁰.

High-resolution soft x-ray studies of $L_{2,3}$ spectra and differentiated spectra for i) Ti in TiO_2 , and in $\text{TiO}_2\text{-HfO}_2$ and ZrO_2 complex oxides, and ii) Sc in LaScO_3 , have been studied in detail. $L_{2,3}$ transitions of TiO_2 terminate in empty 3d states with the 3- and 2-fold degeneracies of the respective $3d_{5/2}$ and $3d_{3/2}$ states completely removed. These removals are attributed to Jahn-Teller distortions in the 6-fold coordinated bonding of Ti to 3-fold coordinated O; Ti-O bond lengths in the z-directions are increased, and the

²⁸ J. L. Whitten et al., J. Vac. Sci. Technol., B 20, 1710 (2002).

²⁹ G. Lucovsky et al., J. Vac. Sci. Technol., B 22, 2132 (2004).

³⁰ V.V. Afanasev and A. Stesmans, in High-k Dielectrics, M. Housa (ed.) (Institute of Physics, Bristol, 2004) Ch.

square in the x-y plane is converted into a rectangle. The Jahn-Teller $3d_{5/2}$ -state *term splittings* in the π -bonded valence bands and their *mirrored conduction band edge image* are quantitatively the same in rutile-structured TiO_2 , and complex $\text{Hf}(\text{Zr})\text{O}_2\text{-TiO}_2$ oxides. This *local interpretation* is confirmed by ab-initio calculations that give term splittings, and relative absorption strengths for the TiO_2 rutile structure. There are significant differences in the $3d_{3/2}$ state σ -bond term splittings between i) TiO_2 , and ii) $\text{TiO}_2\text{-HfO}_2$ and $\text{TiO}_2\text{-ZrO}_2$ complex oxides. These derive from the *central atom* Ti d-states interacting with different combinations of 2nd neighbor Ti, Zr or Hf, d-states through σ -bonding to O p-states. Term splittings have not observed for 4d and 5d states in 3p- and 4p-absorption spectra of ZrO_2 and HfO_2 due to line-width increases associated with short core hole life-times.

π -bonded $3d_{5/2}$ features in Sc $L_{2,3}$ spectra of LaScO_3 are essentially the same in as-deposited films and after annealing to 1000°C , and are qualitatively similar to those of TiO_2 , and TiO_2 complex oxides. Term splittings and relative intensities of the σ -bonded $3d_{3/2}$ features in Sc L_2 spectra are in good agreement with the TiO_2 calculation, but show differences with respect to the TiO_2 spectra that are attributed to 4-fold coordinated O atoms, in contrast to the 3-fold coordination of O in TiO_2 .

D-state related features in O K_1 edges are qualitatively different, and associated with anti-bonding states described in terms of molecular orbitals that *couple* 2nd-neighbor d-states of pairs of TM/RE atoms through π -bonding and σ -bonding with their O neighbors. The *observability* of 5 d^* states is related to the energy separation between d^* and s^* spectral features in elemental oxide O K_1 edges. 3 d^* -state features are observed for $\text{TiO}_2\text{-HfO}_2$ alloys, whereas 5 are found for $\text{TiO}_2\text{-ZrO}_2$. The O K_1 edge of LaAlO_3 displays 5 d^* states, whereas, the O K_1 spectrum of LaScO_3 displays 4 features with the 5th observed in band edge optical and PC spectra^{31,32}.

Bias dependent trapping in conduction band edge states is consistent with trapping into the Jahn-Teller term split states. NEC has recently engineered around this bias dependent trapping by restricting bias levels to ≤ 1.1 eV in stacked $\text{SiO}_2\text{-Hf}$ silicate devices. Bias temperature instabilities (BTI) at higher biases of 1.4 to 1.7 eV have been reported³³, and are consistent with bias dependent trapping into, and release from band edge d^* -states. Finally, since the trapping states are located close to the conduction band edge, there is a marked asymmetry in transport and trapping for substrate and gate injection of electrons. This places significant limitations on the performance and reliability of advanced Si devices as well.

Theoretical Studies

The bonding of transition metal (TM) atoms is qualitatively different in TiO_2 and ZrO_2 , and TM sulfides and selenides, $\text{TiS}(\text{Se})_2$ and $\text{ZrS}(\text{Se})_2$. The Ti and Zr atoms are in

³¹ J.L. Whitten et al., J. Vac. Sci. Technol., B 20, 1710 (2002).

³² V.V. Afanasev and A. Stesmans, in High-k Dielectrics, M. Housa (ed.) (Institute of Physics, Bristol, 2004) Ch.

3.3

³³ J.C. Lee and K. Onishi in Ref. 3, Ch. 5.3.

centro-symmetric 6-fold coordinated octahedral sites in dichalcogenides, and *distorted* 6- and 8(7)-fold coordinated sites in the elemental and complex oxides³⁴. Trivalent lanthanide rare earth (RE) atoms in complex oxides are typically in 12-fold coordinated distorted sites as well. Based on a *molecular orbital* (MO) model³⁵, symmetry differences between oxides and chalcogenides derive in part from differences in π -bonding and σ -bonding MOs connecting pairs of 2nd neighbor TM/RE atoms through $d\pi$ - $p\pi$ - $d\pi$, and $d\sigma$ - $p\sigma$ - $d\sigma$ overlap through *connecting* O atoms. States at the top of TM valence bands are π -bonded and those deeper in the valence band are σ -bonded. Bonding in TM dichalcogenides is predominantly by σ -bonding MOs. These differences in bonding *promote* Jahn-Teller term-splittings (TS) in band valence and conduction d-states of TM/RE elemental and complex oxides.

The MO model has been quantified by ab-initio calculations of valence and conduction band states of Ti atoms in TiO₂ using small clusters centered on either the Ti or O atoms. Ti atoms are bonded to nearest neighbor O atoms terminated by two *shells of charges* that emulate to bonding symmetries and ensure that i) a zero dipole moment for the cluster, and that ii) core levels of nearest-neighbor atom pairs that are correct. The Hamilton is exact for coulomb interactions between electrons and atomic nuclei. Calculations at the self-consistent field Hartree-Fock level are refined variationally at the configuration interaction level to include electron correlation.

The calculated Ti L_{2,3} core 2p absorptions are dipole-allowed *intra-atom* transitions in which the d-state *multiplicities* are determined by valence band $d\pi$ - and $d\sigma$ bonding symmetries. Symmetric arrangements yield transitions to 2 empty d-states: a triply degenerate T_{2g} and doubly degenerate E_g state. *Static* Jahn-Teller *rutile-like* distortions from symmetric bonding completely remove these degeneracies with L_{2,3} transitions terminating in 5 d-states. The 3 d-states derived from the T_{2g} state, are split symmetrically with respect to the degenerate state energy by $\sim 0.75 \pm 0.05$ eV, and 2 E_g states are split symmetrically by ~ 1.2 eV. Calculated TSs and relative transition matrix elements (TMEs) for T_{2g} states are in excellent agreement with experiment for TiO₂, and TiO₂-HfO₂ and TiO₂-ZrO₂ alloys due to the symmetry reductions at Ti sites. However, as a result of different 2nd neighbor contributions Ti 3d σ -bonding at the atom in the center of the cluster, there are significant differences between calculated E_g d-state TSs/RMEs, and experimentally determined σ^* -states for TiO₂, and TiO₂-HfO₂ and TiO₂-ZrO₂ alloys, and these are being addressed.

Based on the MO model, the ab-initio calculations are expected to apply to Sc L_{2,3} transitions of 6-fold coordinated Sc atoms in complex oxides such as LaScO₃ and GdScO₃ as well. Experiments indicate a complete removal of final d-state degeneracies. TSs of the T_{2g} states are reduced by ~ 25 -30% with respect to Ti, but the relative TMEs are about the same. TSs and TMEs for E_g states are in good agreement with calculations based on empty 3d-states alone, but differences between the E_g states of Sc in LaScO₃, and Ti in TiO₂ and the complex oxides are expected on the basis different O atom coordinations: e.g., 3 fold in TiO₂, 4-fold in LaScO₃.

³⁴ L.A. Grunes, Phys. Rev., B 27, 2111 (1983)

³⁵ G. Lucovsky et al., Appl. Phys. Lett., 79, 1775 (2001).

Calculated O K_1 edge spectra for TiO_2 and Ti complex oxides are qualitatively different. Final states are described by MOs constructed from O $2p \pi^*$, and Ti $3d^*$, $4s^*$ and $4p^*$ states. The MO model gives 2 d^* states for symmetric octahedral/dodecahedral sites, and 5 for TM/RE distortions. Similar differences in d^* -state multiplicity are predicted for band edge transitions terminating in the lowest $3d^*$ -conduction band edge states. Observability of 5 d^* -states in ZrO_2 - TiO_2 is reduced to 3 d^* -states in HfO_2 - TiO_2 due to overlap between the higher energy $5d^*$ -states and broader Hf $6s^*$ -states.

3.8.3 Scaling of Si Devices with High-K Gate Dielectrics

The results presented above identify important limitations for the integration of high-k gate dielectrics into advanced Si devices. The necessity for a SiO_2 buffer layer with a self-organized interfacial transition region between the Si substrate and a high gate dielectric places a limitation on the ultimate scaling of EOT. Since this region contributes ~ 0.35 nm to EOT, the lowest values of EOT attainable are ~ 0.8 nm, rather than the roadmap targeted values that extended to 0.5 nm and below.

The mismatch in chemical bonding between the SiO_2 buffer layer and the high-k dielectric requires a second self-organizing at the internal dielectric interface. This restricts the dielectrics than can be used to Zr and Hf oxides, and their respective silicate alloys. The oxides are nano-crystalline when pure, and this leads to Jahn-Teller term splittings of the band edge d^* -states.

Jahn-Teller d^* -state term splittings lead to localized band edge states within the nano-crystallites, and lower energy localized d^* -states from the grain boundaries between the nano-crystallites. These states produce asymmetries in transport and trapping properties that lead to additional limitations on device performance and reliability.

Jahn-Teller term splitting does not occur for the Zr and Hf atoms, respectively, in non-crystalline Zr and Hf silicate alloys, but the performance and reliability of these dielectrics are limited by chemical phase separation that occurs at temperatures of $\sim 900^\circ C$, below the temperatures necessary for activation of dopant atoms in the source and drain regions of the FET devices. This phase separation can be eliminated by nitridation of the silicate alloys, but at the expense of reductions in both device performance and reliability, and more importantly in less aggressively scaling of EOT, to ~ 1 nm. These effects combine to provide only marginal improvements with respect to Si oxynitride devices that at best can be exploited in mobile, battery-operated devices.

3.8.4 Gate Stacks for GaN Devices

Studies of MOS devices with GaN substrates, and the passivation of GaN surfaces in buried channel HEMT and MESFET devices have established that the incorporation of deposited dielectrics in these devices requires separate and independent control of the GaN dielectric interface and the properties of the bulk dielectric. This has demonstrated by separating the processing into three steps: i) formation of an interfacial Ga oxide buffer layer by remote plasma oxidation of GaN, ii) post-oxidation nitridation of this interfacial Ga oxide buffer layer, and iii) deposition of the gate dielectric material. Defect densities in the low 10^{11} cm^{-2} regime have been achieved at the GaN Ga oxide

interface, and fixed charge at the internal dielectric interface is determined by the step in the average bond density, the same scaling parameters as in the Si high-k gate stacks discussed above.

Similar results have been obtained by the Motorola group on GaAs, where the interfacial Ga oxide layer cannot be prepared by oxidation, but instead must be deposited as well. Fixed charge in these devices has been achieved by using Gd gallate as bulk dielectric thereby meeting the bond/atom matching discussed above.

3.9 Defect Characterization in Advanced Semiconductor Devices

3.9.1 Annealing Rate of the Luminescence W-Center in Silicon

The W-Center is one of the dominant radiation-induced defects in silicon found after an additional thermal annealing. Experiments were carried out in order to study the annealing behavior of the W-line in proton-damaged silicon.

Figure 3.9.1 shows the corresponding photoluminescence spectra after the 160°C annealing step of the isochronal annealing procedure ($\Delta t = 15$ min, $\Delta T = 20$ K), for details see: H. Feick and E.R. Weber "Annealing of the photoluminescence W-center in silicon" *Physica B* 273-274 (1999) p. 497. Three materials with vastly different oxygen content are compared. It had already been pointed out that the annealing rate of the W-line does not depend on the impurity content (oxygen, carbon) of the sample. It must therefore be assumed that the defect is entirely composed of intrinsic lattice defects. It is then interesting to study how the annealing rate changes when the density of intrinsic defects is varied.

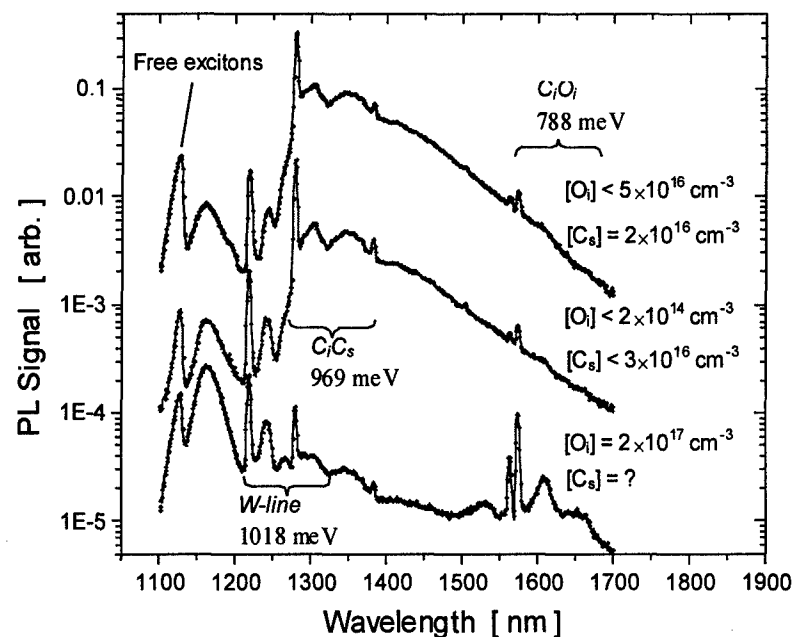


Figure 3.9.1: Photoluminescence spectra of silicon irradiated with 55 MeV protons to a fluence of $5 \times 10^{11} \text{ cm}^{-2}$. Three different materials with largely different oxygen content are compared after 15 min annealing at 160°C.

Figure 3.9.2 shows the strength of the luminescence as function of the annealing temperature for 6 samples irradiated with proton fluences of 3×10^{13} and 5×10^{11} cm^{-2} , respectively. In order to allow for a comparison of the annealing behavior the data have been normalized with respect to the data at 160C. Although there is a significant scatter in the data it can be seen that the annealing of the W-line is slower for the lower proton dose. A possible explanation would be that the defect is formed by the diffusion-limited reaction of two components.

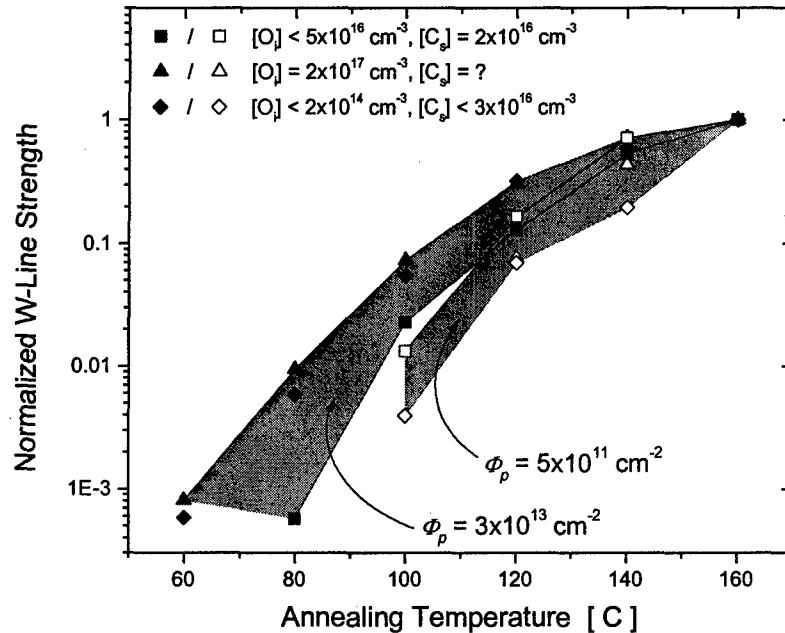


Figure 3.9.2: Annealing rate of the W-line compared at two different proton doses. The data have been normalized with respect to the luminescence intensity of the line after the 160C annealing step.

3.9.2 Electron Ionization Damage in Ultrathin Zirconium Dielectrics

Experiments were carried out on advanced Zr-based dielectrics (ZrSiO_4 and ZrO_2) to determine the Radiation-Induced Leakage Current (RILC). The devices were 100 μm square NMOS capacitors with an equivalent oxide thickness of 10 \AA . The results were compared to NMOS capacitors with an ultrathin (20 \AA) SiO_2 gate dielectric. The devices were irradiated with 20 keV electrons in an SEM at a dose rate of approximately 42.8 krad(Si)/min, up to final doses of 50, 100, 250, 500, and 750 krad(Si). No stress was applied during irradiation.

RILC was primarily observed in irradiated devices at $V_g > 0.5$ V for the Zr-based dielectrics and at $V_g > 0.3$ V for SiO_2 . Saturation of the RILC was observed after a dose of 100 krad for the ZrSiO_4 and ZrO_2 dielectrics. In addition, the IV curves show an absence of a Fowler-Nordheim current region up to $V_g = 4$ V.

Figure 3.9.3 shows the radiation-induced leakage current versus dose. To calculate the excess leakage current we took the current value at 4V, where the IV curve had leveled off, and subtracted the pre-irradiation value from each of the irradiated curves. The CV curves for the Zr based dielectrics did not show any shift.

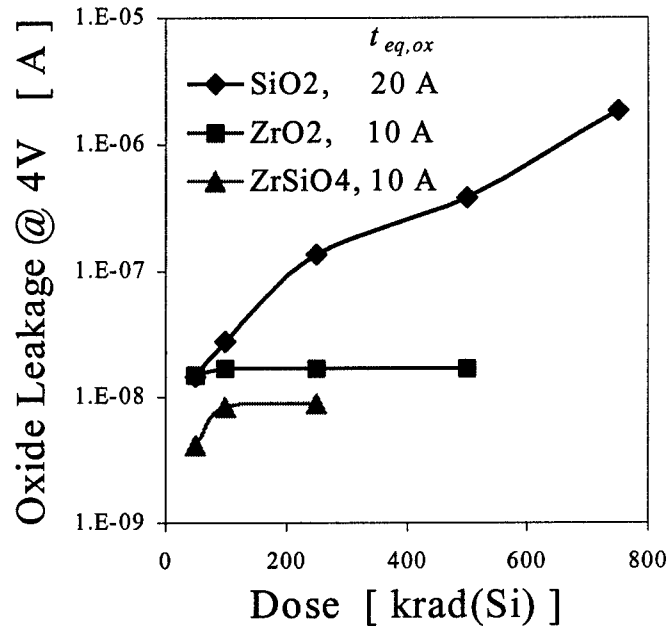


Figure 3.9.3: RILC of Zr-based ultrathin dielectrics.

3.9.3 Defects Related to Nitrogen Sublattice Damage in Electron Irradiated GaN

Radiation damage studies of GaN provide insights into the fundamental properties of the material as well as the basic knowledge needed to predict degradation of GaN-based devices in space-based applications or other radiation environments. Our focus is on the luminescence properties of these materials, which are characterized with time-resolved and continuous-wave excitation.

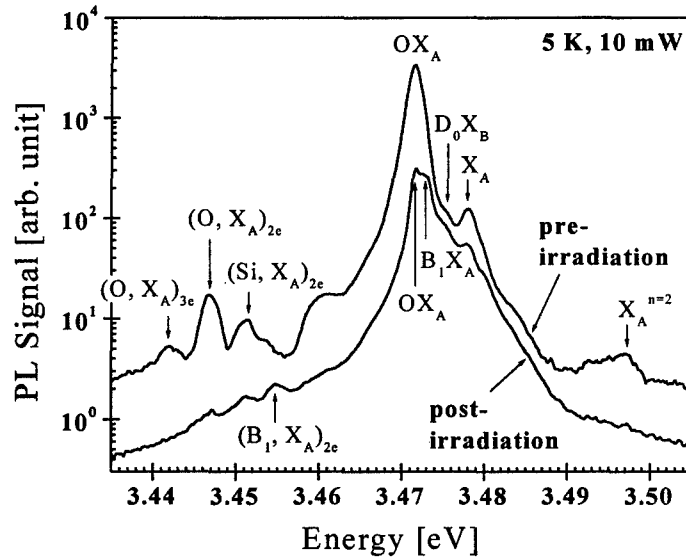


Figure 3.9.4: Time-integrated luminescence spectra of the 250 μm free-standing Samsung HVPE GaN before and after 0.42 MeV electron irradiation.

High quality free-standing HVPE GaN samples grown by Samsung Advanced Institute of Technology were irradiated with electrons at Hanscome AFB. The electron energy was chosen to be 0.42 MeV because electrons with this energy damage exclusively the N-sublattice of GaN. After irradiation two new luminescence lines at 3.4733 eV and 3.4543 eV were detected by time-resolved photoluminescence (TRPL) (Figure 3.9.4). The two lines were associated with the ground state bound exciton of a new donor B_1 and its two-electron transition. The donor binding energy of B_1 was determined as 24.7 ± 0.4 meV, shallower than the donors O_N and Si_{Ga} . Among the possible defects, nitrogen vacancy (V_N) was the best candidate for the new donor B_1 .

In addition, a change under focused 267 nm laser beam was observed at low temperature in the excitonic luminescence of the irradiated sample. The oxygen-bound exciton intensity, the total band edge luminescence intensity, and the luminescence decay lifetime of free and bound excitons all increased with laser exposure time. In contrast, the relative intensity of the two new lines related to B_1 decreased. Finally a stable state was reached. The rate to reach the stable state decreased with increasing laser power. The change under laser illumination was not observed with below bandgap illumination. We propose that the change reflects the light-induced dissociation of the non-radiative defect complex N_i-O_N and subsequently the migration of N_i and at least partial annihilation of N_i with V_N .

Isochronal annealing of 15 minutes was carried out from 50°C to 600°C. Figure 3.9.5 shows the spectral evolution upon annealing. B_1 -bound exciton emission starts to disappear after 300°C annealing, and is completely gone after annealing at 350°C. No further change is observed from 350°C to 600°C. In addition, the laser induced change no longer exists after 350°C annealing, corresponding to the disappearance of B_1 -bound exciton emission. The annealing study indicates that the V_N-N_i Frenkel pairs annihilate above 300°C. This also suggests that above 300°C the proposed N_i-O_N

complexes can effectively dissociate and the N_i becomes mobile (consistent with the 1.5-2.5 eV migration barrier).

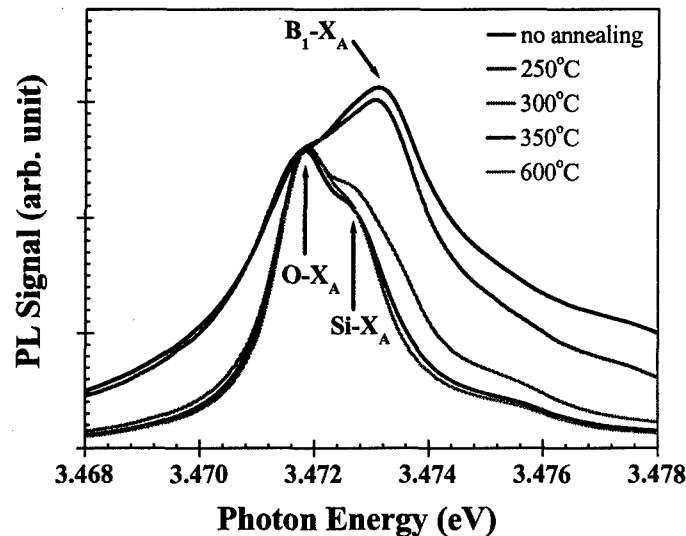


Figure 3.9.5: Time-integrated PL spectra after annealing. All spectra were measured at 11K, 10mW and with 4 seconds laser exposure.

3.9.4 Evaluation of Radiation Hardness of GaN

Table 3.9.1: Lifetime degradation constants for different GaN layers irradiated with 25 and 55 MeV protons.

| GaN Sample | 160- μm HVPE | 10- μm HVPE on Sapphire | MBE G652 | MBE G644 |
|--|----------------------------|--|---------------------|---------------------|
| K_τ [cm^2 / ns] | 4×10^{-15} | 2×10^{-14} | 8×10^{-15} | 4×10^{-15} |
| τ (ps), pre-irradiation | 1049 | 160 | 208 | 240 |

From the difference between the inverse lifetime values before and after irradiation, we can estimate the lifetime degradation constants for GaN. These values are listed in Table I for different GaN layer irradiated with 25 MeV and 55 MeV protons. Generally, a much lower amount of structural defects is expected for the thick HVPE layer. The MBE overgrowth layer generally replicates the structural quality of the template; some improvements are possible due to growth conditions closer to perfect stoichiometry. This trend is indeed observed in the carrier lifetimes measured before irradiation. A very large value of about 1 ns was observed for the thick HVPE layer, while the thin HVPE layer and the MBE overgrown layer displayed values of about 160 ps and 210 ps, respectively. It is seen from Table I that smaller lifetime degradation constant correlates with longer lifetime of the undamaged material.

Therefore, it is suggested that structural defects facilitate the formation of the radiation-induced lifetime killer defects. This finding is in agreement with the more pronounced quenching of the cw-luminescence observed in the thin layers compared with the 160 μm thick HVPE layer.

In Figure 3.9.6 we compare the lifetime degradation constant K_τ of GaN and GaAs. K_τ is about 5 to 25 times smaller than the values reported for GaAs irradiated with protons of similar energy³⁶.

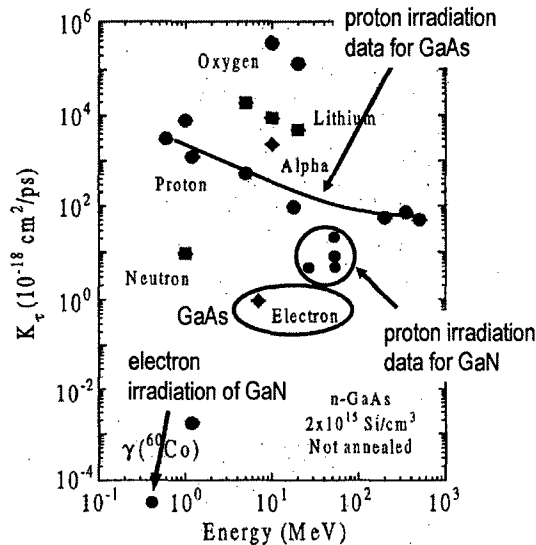


Figure 3.9.6: Comparison of lifetime degradation constants K_τ between GaN and GaAs³⁶.

3.9.5 Radiation Tolerance of GaAs-On-Insulator MESFETs

The Berkeley group studied proton damage effects in GaAs-On-Insulator (GOI) MESFETs, for which the insulating buffer layer is produced by wet lateral oxidation of aluminum arsenide buffer layers. This relates as well to other application as of laterally oxidized AlAs, for example as current confinement layers in vertical-cavity surface emitting lasers (VCSELs). Carrying out the oxidation process longer than needed to achieve full lateral oxidation of the AlAs layer (over-oxidation) is found to have deleterious effects on device performance. Not only the radiation tolerance of this relatively novel technology is widely unknown, but also its dependence on the oxidation process has never been reported.

Devices were obtained through the collaboration with the MURI at the University of California, Santa Barbara. A chief benefit of this technology is the reduced buffer leakage, resulting in record power added efficiencies. In order to explore systematically the radiation tolerance of the Al_2O_3 layer and the interface with GaAs, we fabricated GOI MESFETs with different oxidation times as well as standard GaAs reference MESFETs at the UC Berkeley Microfabrication Laboratory. GOI MESFETs with different gate widths of 40, 100, and 300 μm were fabricated resulting in different over-oxidation times for the AlAs layer. The oxidation was carried out for 80 minutes

³⁶ M. Parenteau, C. Carlone, D. Morris, S. M. Khanna, IEEE Trans. Nucl. Sci. 44, 1849 (1997).

with the goal of just completely oxidizing the widest (300 μm) device. Consequently, the 40 μm gate width devices are heavily over-oxidized. Device DC characteristics of various GOI MESFETs and standard reference MESFETs were studied before and after 55 MeV proton irradiations with the fluences 5.4×10^{12} , 1.62×10^{13} , 3×10^{13} , and $6 \times 10^{13} \text{ cm}^{-2}$. For device performance and defect characterization, low-frequency noise measurements were also carried out.

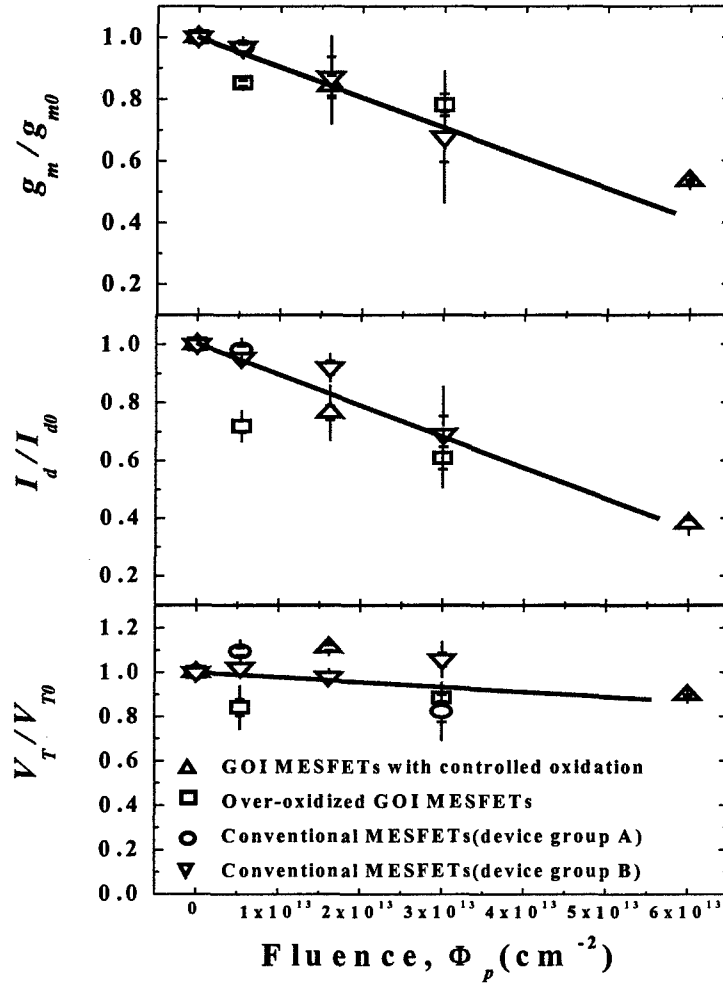


Figure 3.9.7: Variation of the drain current I_d , transconductance g_m , and threshold voltage V_T with 55 MeV proton irradiation fluence for GaAs-On-Insulator and conventional MESFETs.

Figure 3.9.7 shows the variation of the drain current I_d , transconductance g_m , and threshold voltage V_T with proton fluence on conventional reference MESFETs and GOI MESFETs with different over-oxidation. For each device, the measured parameters were normalized with respect to the value measured before irradiation on the same device. The vertical error bar designates the standard deviation within the set of devices studied, and the horizontal bar indicates the uncertainty of the average. All the devices showed similar fluence dependence. Drain current and transconductance, both taken at zero gate bias, degrade with proton fluence. Within the given errors, the transconductance reduction with fluence is equal to the drain current reduction.

Moreover, the threshold voltage remains almost unchanged upon irradiation, with perhaps a small increase. The fluence dependence seems to indicate that the displacement damage of 55 MeV proton irradiation is dominated by mobility reduction and it is independent of buffer oxidation conditions. From the DC characteristics, MESFETs using GOI technology have similar radiation hardness as conventional MESFETs and the radiation hardness does not change with different amounts of over-oxidation.

Nevertheless, the low-frequency noise measurement shown in Figure 3.9.8 reveals a fluence dependence that is absent in DC characteristic in the present proton-fluence range. The $1/f$ noise spectral density is normalized with the square of the current to compare devices with different widths. The fluctuation of the data depends significantly on different fabrication runs even with identical process flow. However, the $1/f$ noise component clearly shows a higher noise level on GOI MESFETs and more degradation with radiation than conventional MESFETs. Its radiation sensitivity is strongly dependent on amount of over-oxidation.

The mechanism of $1/f$ noise is not yet clear. Even though a detailed model is indeed needed to completely understand the $1/f$ noise mechanism, the obvious radiation sensitivity dependence on the amount of over oxidation is already revealed.

From generation-recombination (g-r) noise components, many trap levels could be resolved depending on fluence and over-oxidation. In pre-irradiated samples, three levels were revealed at $E_C - 0.7$ eV, $E_C - 0.47$ eV, and $E_C - 0.32$ eV. The mid-gap trap is identical to EB4, a complex associated with As_{Ga} , in both energy level and cross section. The level at 0.47 eV, appearing only at larger gate biases, may be related to surface conduction processes. In 55 MeV proton-irradiated samples, levels at $E_C - 0.79$ eV, $E_C - 0.63$ eV, and $E_C - 0.54$ eV, and $E_C - 0.26$ eV were observed. A zoo of defects observed after 55 MeV proton irradiation can be well correlated to the fluence dependence of $1/f$ noise component, for which one of its physical origin is carrier number fluctuation.

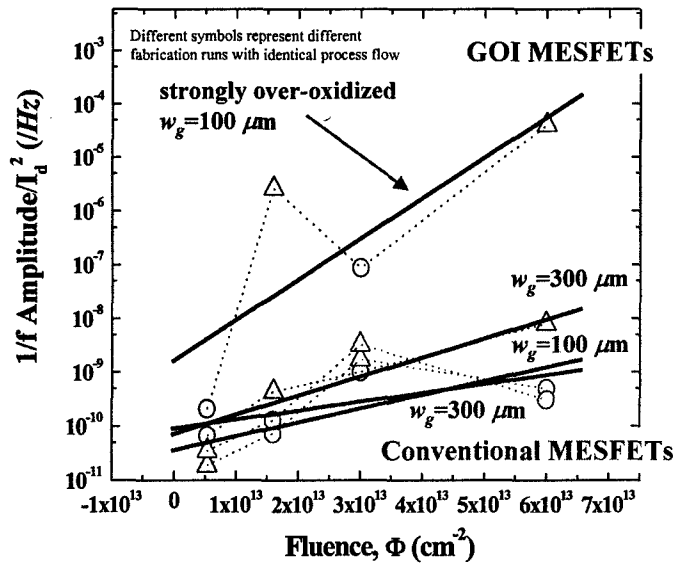


Figure 3.9.8: Fluence dependence of $1/f$ noise component for GaAs-On-Insulator and conventional MESFETs.

3.9.6 Radiation Effects in AlGaIn/GaN Heterostructure Transistors

AlGaIn/GaN heterostructure transistors were provided by UC Santa Barbara and were also exposed to a fluence of $3 \times 10^{13} \text{ cm}^{-2}$. On these devices we studied the current-voltage and capacitance-voltage characteristics of the gate diode, see Figure 3.9.9. The reverse as well as the forward current is found to be reduced after the proton exposure, indicating a change in the barrier height of the diode. The radiation-induced drop in the capacitance indicates a loss of channel charge, which again probably is due to compensation by radiation-induced deep levels. Also a noteworthy shift in the threshold voltage is observed.

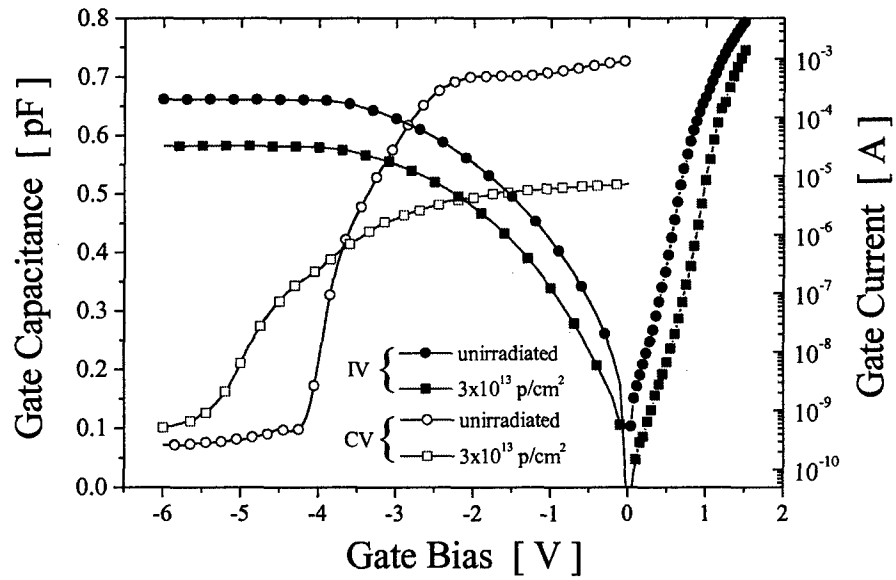


Figure 3.9.9: Current-voltage (IV) and capacitance-voltage (CV) characteristics of the gate diode of an AlGaIn/GaN heterostructure transistor before and after exposure to 55 MeV protons.

4 PERSONNEL SUPPORTED

Vanderbilt University

- Ron Schrimpf, Professor
- Sokrates Pantelides, Professor
- Norm Tolk, Professor
- Dan Fleetwood, Professor
- Lloyd Massengill, Professor
- Sergey Rashkeev, Research Professor
- Claude Cirba, Senior Research Associate
- Paul Bunson, Senior Research Associate
- Bongim Jun, Senior Research Associate
- Sungchul Lee, Senior Research Associate
- Bo Choi, Senior Research Associate
- Yuanfu Zhao, Senior Research Associate
- Leonidas Tsetseris, Research Associate
- Tamas Bakos, Graduate Student
- Robert Pasternak, Graduate Student
- Z. Marka, Graduate Student
- Ajay Raparla, Graduate Student
- Xinwen Hu, Graduate Student
- James Felix, Graduate Student
- Hao Xiong, Graduate Student
- Aditya Karmarkar, Graduate Student
- Amitabh Chatterjee, Graduate Student
- Xing Zhou, Graduate Student

- Mandy Conley, Staff
- Connie Nichols, Staff

North Carolina State University

- Gerry Lucovsky, Professor
- Yi Mu Lee, Graduate Student

Ohio State University

- Len Brillson, Professor
- Brad D. White, Graduate Student

University of California–Berkeley

- Eicke R. Weber, Professor
- Qing Yang, Graduate Student

University of Arizona

- Mark A. Neifeld, Professor
- Aditya Kalavagunta, Graduate Student

5 PUBLICATIONS

S. N. Rashkeev, D. M. Fleetwood, R. D. Schrimpf, and S. T. Pantelides, "Effects of hydrogen motion on interface trap formation and annealing," *IEEE Trans. Nucl. Sci.* **51**, 3158-3165 (2004).

1. H. D. Xiong, B. Jun, D. M. Fleetwood, R. D. Schrimpf, and J. R. Schwank, "Charge trapping and low frequency noise in SOI buried oxides," *IEEE Trans. Nucl. Sci.* **51**, 3238-3242 (2004).
2. J. A. Felix, M. R. Shaneyfelt, D. M. Fleetwood, J. R. Schwank, P. E. Dodd, E. P. Gusev, R. M. Fleming, and C. D'Emic, "Charge trapping and annealing in high- κ gate dielectrics," *IEEE Trans. Nucl. Sci.* **51**, 3143-3149 (2004).
3. J. W. Stacey, R. D. Schrimpf, D. M. Fleetwood, and K. C. Holmes, "Using surface charge analysis to characterize the radiation response of Si/SiO₂ structures," *IEEE Trans. Nucl. Sci.* **51**, 3686-3691 (2004).
4. B. Jun, R. D. Schrimpf, D. M. Fleetwood, Y. V. White, R. Pasternak, S. N. Rashkeev, F. Brunier, N. Bresson, M. Fouillat, S. Cristoloveanu, and N. H. Tolk, "Charge trapping in irradiated SOI wafers measured by second harmonic generation," *IEEE Trans. Nucl. Sci.* **51**, 3231-3237 (2004).
5. A. P. Karmarkar, B. Jun, D. M. Fleetwood, R. D. Schrimpf, R. A. Weller, B. D. White, L. J. Brillson, and U. K. Mishra, "Proton irradiation effects on GaN-based high electron mobility transistors with Si-doped Al_xGa_{1-x}N and thick GaN cap layers," *IEEE Trans. Nucl. Sci.* **51**, 3801-3806 (2004).
6. B. Jun, H. D. Xiong, A. L. Sternberg, C. R. Cirba, D. Chen, R. D. Schrimpf, D. M. Fleetwood, J. R. Schwank, and S. Cristoloveanu, "Total dose effects on double gate fully depleted SOI MOSFETs," *IEEE Trans. Nucl. Sci.* **51**, 3767-3772 (2004).
7. L. Tsetseris, X. J. Zhou, D. M. Fleetwood, R. D. Schrimpf, and S. T. Pantelides, "Dual role of fluorine at the Si-SiO₂ interface," *Appl. Phys. Lett.* **85**, 4950-4952 (2004).
8. B. Jun, Y. V. White, R. D. Schrimpf, D. M. Fleetwood, F. Brunier, N. Bresson, S. Cristoloveanu, and N. H. Tolk, "Characterization of multiple Si/SiO₂ interfaces in silicon-on-insulator materials via second-harmonic generation," *Appl. Phys. Lett.* **85**, 3095-3097 (2004).
9. B. Jun, M. Fouillat, R. D. Schrimpf, D. M. Fleetwood, and S. Cristoloveanu, "Total dose radiation effects in partially-depleted SOI transistors with ultrathin gate oxide," *Proceedings IEEE SOI Conference*, Charleston SC, October 4-7, 2004, pp. 30-31.
10. S. N. Rashkeev, D. M. Fleetwood, R. D. Schrimpf, and S. T. Pantelides, "Hydrogen at the Si/SiO₂ Interface: From Atomic-Scale Calculations to Engineering Models," in *Radiation Effects and Soft Errors in Integrated Circuits and Electronic Devices*, edited by R. D. Schrimpf and D. M. Fleetwood (World Scientific, Singapore, 2004), pp. 291-296.

11. C. R. Cirba, J. A. Felix, K. F. Galloway, R. D. Schrimpf, D. M. Fleetwood, and S. Cristoloveanu, "Space-radiation effects in advanced SOI devices and alternative gate dielectrics," in *Future Trends in Microelectronics: the Nano, the Giga, and the Ultra*, eds. S. Luryi, J. Xu, and A. Zaslavsky (Wiley, New York, 2004), pp. 115-126.
12. H. D. Xiong, D. M. Fleetwood, and J. R. Schwank, "Low-frequency noise and radiation response of buried oxides in SOI nMOS transistors," *IEE Proc. Circuits, Devices & Systems* **151**, 118-124 (2004).
13. X. J. Zhou, L. Tsetseris, S. N. Rashkeev, D. M. Fleetwood, R. D. Schrimpf, S. T. Pantelides, J. A. Felix, E. P. Gusev, and C. D'Emic, "Negative bias-temperature instabilities in MOS devices with SiO₂ and SiO_xN_y/HfO₂ gate dielectrics," *Appl. Phys. Lett.* **84**, 4394-4396 (2004).
14. J. A. Felix, H. D. Xiong, D. M. Fleetwood, E. P. Gusev, R. D. Schrimpf, A. L. Sternberg, and C. D'Emic, "Interface trapping properties of nMOSFETs with Al₂O₃/SiO_xN_y/Si (100) gate dielectric stacks after exposure to ionizing radiation," *Microelectron. Engrg.* **72**, 50-54 (2004).
15. J. A. Felix, J. R. Schwank, C. R. Cirba, R. D. Schrimpf, M. R. Shaneyfelt, D. M. Fleetwood, and P. E. Dodd, "Influence of total-dose radiation on the electrical characteristics of SOI MOSFETs," *Microelectron. Engrg.* **72**, 332-341 (2004). [Invited.]
16. X. Hu, B. K. Choi, H. J. Barnaby, D. M. Fleetwood, R. D. Schrimpf, S. C. Lee, S. Shojah-Ardalan, R. Wilkins, U. K. Mishra, and R. Dettmer, "The Energy Dependence of Proton-Induced Degradation in AlGaIn/GaN High Electron Mobility Transistors," *IEEE Trans. Nucl. Sci.* **51**, 293-297 (2004) [also in RADECS2002 Workshop Proc., pp. 17-20, 2002].
17. J. A. Felix, J. R. Schwank, D. M. Fleetwood, M. R. Shaneyfelt, and E. P. Gusev, "Effects of radiation and charge trapping on the reliability of high- κ gate dielectrics," *Microelectron. Reliab.* **44**, 563-575 (2004). [Invited.]
18. S.T. Bradley, L.J. Brillson, J. Hwang, and W.J. Schaff, "Surface Cleaning and Annealing Effects on Ni/AlGaIn Interface Atomic Composition and Schottky Barrier Height," *Applied Physics Letters* vol. 85, 1368-1370 (2004).
19. X. L. Sun, S. T. Bradley, G. H. Jessen, D. C. Look, R. J. Molnar, and L. J. Brillson, "Micro-Auger Electron Spectroscopy Studies of Chemical and Electronic Effects at GaN-Sapphire Interfaces," *Journal of Vacuum Science and Technology*, vol. 22, 2284-2289 (2004).
20. A. Kalavagunta, R. Schrimpf, and M. A. Neifeld, "Design considerations for optical systems in ionizing and nonionizing radiation environments," *IEEE Transactions on Nuclear Science*, Vol.51, pp.3595-3602, December, 2004.
21. J. A. Felix, M. R. Shaneyfelt, D. M. Fleetwood, T. L. Meisenheimer, J. R. Schwank, R. D. Schrimpf, P. E. Dodd, E. P. Gusev, and C. D'Emic, "Radiation-induced charge trapping

- in thin $\text{Al}_2\text{O}_3/\text{SiO}_x\text{N}_y/\text{Si}(100)$ gate dielectric stacks," *IEEE Trans. Nucl. Sci.* **50**, 1910-1918 (2003).
22. B. Jun, D. M. Fleetwood, R. D. Schrimpf, X. J. Zhou, E. J. Montes, and S. Cristoloveanu, "Charge separation techniques for irradiated pseudo-MOS SOI transistors," *IEEE Trans. Nucl. Sci.* **50**, 1891-1895 (2003).
 23. S. N. Rashkeev, D. M. Fleetwood, R. D. Schrimpf, and S. T. Pantelides, "Statistical modeling of radiation-induced proton transport in Si: deactivation of dopant acceptors in bipolar devices," *IEEE Trans. Nucl. Sci.* **50**, 1896-1900 (2003).
 24. X. Hu, A. P. Karmarkar, B. Jun, D. M. Fleetwood, R. D. Schrimpf, R. D. Geil, R. A. Weller, B. D. White, M. Bataiev, L. J. Brillson, and U. K. Mishra, "Proton irradiation effects on AlGaIn/AlN/GaN high electron mobility transistors," *IEEE Trans. Nucl. Sci.* **50**, 1791-1796 (2003).
 25. B. D. White, M. Bataiev, S. H. Goss, X. Hu, A. Karmarkar, D. M. Fleetwood, R. D. Schrimpf, W. J. Schaff, and L. J. Brillson, "Electrical, spectral, and chemical properties of 1.8 MeV proton irradiated AlGaIn/GaN HEMT structures as a function of proton fluence," *IEEE Trans. Nucl. Sci.* **50**, 1934-1941 (2003).
 26. R. Pasternak, A. Chatterjee, Y. V. Shirovkaya, B. K. Choi, Z. Marka, J. K. Miller, R. G. Albridge, S. N. Rashkeev, S. T. Pantelides, R. D. Schrimpf, D. M. Fleetwood, and N. H. Tolk, "Contactless ultra-fast laser probing of radiation-induced leakage current in ultra-thin oxides," *IEEE Trans. Nucl. Sci.* **50**, 1929-1933 (2003).
 27. H. D. Xiong, D. M. Fleetwood, J. A. Felix, E. P. Gusev, and C. D'Emic, "Low-Frequency Noise and Radiation Response of MOS Transistors with $\text{Al}_2\text{O}_3/\text{SiO}_x\text{N}_y/\text{Si}(100)$ Gate Stacks," *Appl. Phys. Lett.* **83**, 5232-5234 (2003).
 28. S. N. Rashkeev, D. M. Fleetwood, R. D. Schrimpf, and S. T. Pantelides, "Radiation-Induced Acceptor Deactivation in Bipolar Devices: Effects of Electric Field," *Appl. Phys. Lett.* **83**, 4646-4648 (2003).
 29. L. Tsetseris, X. Zhou, D. M. Fleetwood, R. D. Schrimpf, and S. T. Pantelides, "Field-Induced Reactions of Water Molecules at Si-Dielectric Interfaces," E3.3, *MRS Proc.* **786**, Boston, MA (2003).
 30. Y. Jiang, R. Pasternak, Z. Marka, Y. V. Shirovkaya, J. K. Miller, S. N. Rashkeev, Yu. D. Glinka, I. E. Perakis, P. K. Roy, J. Kozub, B. K. Choi, D. M. Fleetwood, R. D. Schrimpf, X. Liu, Y. Sasaki, J. K. Furdyna, and N. H. Tolk, "Spin/Carrier Dynamics at Semiconductor Interfaces Using Intense, Tunable Ultra-Fast Lasers," *Phys. Stat. Sol. (b)* **240**, 490-499 (2003).
 31. R. Pasternak, Y. V. Shirovkaya, Z. Marka, J. K. Miller, S. N. Rashkeev, S. T. Pantelides, N. H. Tolk, B. K. Choi, R. D. Schrimpf, and D. M. Fleetwood, "Laser Detection of Radiation Enhanced Electron Transport in Ultra-Thin Oxides," *Nucl. Instrum. Meth. Phys. Res. A* **514**, 150-155 (2003).

32. D. M. Fleetwood, "Microstructures of Defects Causing Noise in MOS Devices," in *Noise as a Tool for Studying Materials*, edited by M. B. Weissman, N. E. Israeloff, and S. Kogan (Proc. SPIE Vol. 5112), pp. 259-270 (2003). [Invited.]
33. H. D. Xiong, D. M. Fleetwood, and J. R. Schwank, "Low Frequency Noise and Radiation Response of Buried Oxides in SOI nMOS Transistors," in *Noise in Devices and Circuits*, edited by M. J. Deen, Z. Celik-Butler, and M. E. Levinstein (Proc. SPIE Vol. 5113), pp. 44-55 (2003). [Invited.]
34. D. M. Fleetwood, S. N. Rashkeev, Z. Y. Lu, C. J. Nicklaw, J. A. Felix, R. D. Schrimpf, and S. T. Pantelides, "Dipoles in SiO₂: Border Traps or Not?," PV 2003-02 Silicon Nitride and Silicon Dioxide Thin Insulating Films (7th), edited by R. E. Sah, K. B. Sunda, J. Deen, D. Landheer, W. D. Brown, and D. Misra (The Electrochemical Society, Pennington, NJ), pp. 291-307 (2003). [Invited.]
35. C. R. Cirba, S. Cristoloveanu, R. D. Schrimpf, L. C. Feldman, D. M. Fleetwood, and K. F. Galloway, "Total-Dose Radiation Hardness of Double-Gate Ultra-Thin SOI MOSFETs," PV 2003-05 Silicon-on-Insulator Technology and Devices XI, edited by S. Cristoloveanu, G. K. Celler, J. G. F. Gamiz, K. Izumi, and Y. W. Kim (The Electrochemical Society, Pennington, NJ), pp. 493-498 (2003).
36. V. A. K. Raparla, S. C. Lee, R. D. Schrimpf, D. M. Fleetwood, and K. F. Galloway, "A Model of Radiation Effects in Nitride-Oxide Films for Power MOSFET Applications," *Solid-St. Electron.* **47**, 775-783 (2003).
37. Z. Marka, R. Pasternak, R. G. Albridge, S. N. Rashkeev, S. T. Pantelides, N. H. Tolk, B. K. Choi, D. M. Fleetwood, and R. D. Schrimpf (VU), "Two-Color Optical Technique for Characterization of X-ray Radiation-Enhanced Electron Transport in SiO₂," *J. Appl. Phys.* **93**, 1865-1870 (2003).
38. Z. Marka, R. Pasternak, S.N. Rashkeev, S. T. Pantelides, N. H. Tolk, P.K. Roy, J. Kozub, "Band Offsets Measured by Internal Photoemission Induced Second-Harmonic Generation," *Physical Review B*, **67**, 045302, 2003.
39. G.H. Jessen, R.C. Fitch, J. K. Gillespie, G.D. Via, B.D. White, S.T. Bradley, D.E. Walker Jr., and L.J. Brillson, "The Effects of Deep Level Defects on Ohmic Contact and Frequency Performance of AlGaIn/GaN HEMTs," *Applied Physics Letters*, vol. 83, 485-487 (2003).
40. S. T. Bradley, S. H. Goss, and L. J. Brillson, "Deep Level Defects and Doping in High Al Mole Fraction AlGaIn," *Journal of Vacuum Science and Technology*, vol. 21, 558-2563 (2003).
41. L.J. Brillson, "Microcathodoluminescence Characterization of III-V Nitride Heterojunctions and Devices," *Wide Band Gap Semiconductors for Photonic Devices and Sensors III*, ed. E.B. Stokes, R.C. Fitch, Jr., D.N. Buckley, P.C. Chang, D.W. Merfeld, and F. Ren (The Electrochemical Society, Pennington, NY, 2003) pp.. 229-235.

42. A. Kalavagunta, B. Choi, M. A. Neifeld, and R. Schrimpf, "Effects of 2 MeV proton irradiation on operating wavelength and leakage current of vertical cavity surface emitting lasers," *IEEE Transactions on Nuclear Science*, Vol.50, pp.1982-1991, 2003.
43. Z. Y. Lu, C. J. Nicklaw, D. M. Fleetwood, R. D. Schrimpf, and S. T. Pantelides, "Structure, Properties, and Dynamics of Oxygen Vacancies in Amorphous SiO₂," *Phys. Rev. Lett.* **89**, 285505-1 to 285505-4 (2002).
44. D. M. Fleetwood, H. D. Xiong, Z. Y. Lu, C. J. Nicklaw, J. A. Felix, R. D. Schrimpf, and S. T. Pantelides, "Unified Model of Hole Trapping, 1/f Noise, and Thermally Stimulated Current in MOS Devices," *IEEE Trans. Nucl. Sci.* **49**, 2674-2683 (2002). ***Meritorious Conference Paper Award, 2002 IEEE Nuclear and Space Radiation Effects Conference.***
45. H. D. Xiong, D. M. Fleetwood, B. K. Choi, and A. L. Sternberg, "Temperature Dependence and Irradiation Response of 1/f Noise in MOSFETs," *IEEE Trans. Nucl. Sci.* **49**, 2718-2723 (2002).
46. J. A. Felix, D. M. Fleetwood, R. D. Schrimpf, J. G. Hong, G. Lucovsky, J. R. Schwank, and M. R. Shaneyfelt, "Total Dose Radiation Response of Hafnium Silicate Capacitors," *IEEE Trans. Nucl. Sci.* **49**, 3191-3196 (2002).
47. S. N. Rashkeev, C. R. Cirba, D. M. Fleetwood, R. D. Schrimpf, S. C. Witzak, A. Michez, and S. T. Pantelides, "Physical Model for Enhanced Interface-Trap Formation at Low Dose Rates," *IEEE Trans. Nucl. Sci.* **49**, 2650-2655 (2002). ***Meritorious Conference Paper Award, 2002 IEEE Nuclear and Space Radiation Effects Conference.***
48. B. K. Choi, D. M. Fleetwood, R. D. Schrimpf, L. W. Massengill, K. F. Galloway, M. R. Shaneyfelt, T. L. Meisenheimer, P. E. Dodd, J. R. Schwank, Y. M. Lee, R. S. Johnson, and G. Lucovsky, "Long-Term Reliability Degradation of Ultra-Thin Dielectric Films due to Heavy-Ion Irradiation," *IEEE Trans. Nucl. Sci.* **49**, 3045-3050 (2002).
49. C. J. Nicklaw, Z. Y. Lu, D. M. Fleetwood, R. D. Schrimpf, and S. T. Pantelides, "The Structure, Properties, and Dynamics of Oxygen Vacancies in Amorphous SiO₂," *IEEE Trans. Nucl. Sci.* **49**, 2667-2673 (2002).
50. X. Hu, B. K. Choi, H. J. Barnaby, D. M. Fleetwood, R. D. Schrimpf, K. F. Galloway, R. A. Weller, K. McDonald, U. K. Mishra, and R. Dettmer, "Proton-Induced Degradation in AlGaAs/GaAs Heterojunction Bipolar Transistors," *IEEE Trans. Nucl. Sci.* **49**, 3213-3216 (2002).
51. B. D. White, M. Bataiev, L. J. Brillson, B. K. Choi, D. M. Fleetwood, R. D. Schrimpf, S. T. Pantelides, R. W. Dettmer, W. J. Schaff, J. G. Champlain, and U. K. Mishra, "Characterization of 1.8 MeV Proton Irradiated AlGaN/GaN Field-Effect Transistor Structures by Nanoscale Depth-Resolved Luminescence Spectroscopy," *IEEE Trans. Nucl. Sci.* **49**, 2695-2701 (2002).

52. B. D. White, L. J. Brillson, M. Bataiev, D. M. Fleetwood, R. D. Schrimpf, B. K. Choi, and S. T. Pantelides, "Detection of Trap Activation by Ionizing Radiation in SiO₂ by Spatially Localized Cathodoluminescence Spectroscopy," *J. Appl. Phys.* **92**, 5729-5734 (2002).
53. D. M. Fleetwood, "Hydrogen-Related Reliability Issues for Advanced Microelectronics," *Microelectron. Reliab.* **42**, 1397-1403 (2002). [Invited.]
54. S. N. Rashkeev, D. M. Fleetwood, R. D. Schrimpf, and S. T. Pantelides, "Dual Behavior of H⁺ at Si-SiO₂ Interfaces: Mobility versus Trapping," *Appl. Phys. Lett.* **81**, 1839-1841 (2002).
55. D. M. Fleetwood, "Effects of Hydrogen Transport and Reactions on Microelectronics Radiation Response and Reliability," *Microel. Reliab.* **42**, 523-541 (2002). [Invited.]
56. C. R. Cirba, H. J. Barnaby, J. M. Hutson, J. A. Felix, R. D. Schrimpf, and D. M. Fleetwood, "Modeling Oxide Trapped Charge Annealing Processes in Irradiated SOI MOSFETs," *GOMAC Technical Digest*, pp. 496-99 (2002).
57. B. K. Choi, D. M. Fleetwood, L. W. Massengill, R. D. Schrimpf, K. F. Galloway, M. R. Shaneyfelt, T. L. Meisenheimer, P. E. Dodd, J. R. Schwank, Y. M. Lee, R. S. Johnson, and G. Lucovsky, "Reliability Degradation of Ultrathin oxynitride and Al₂O₃ Gate Dielectric Films Owing to Heavy-Ion Irradiation," *Electronics Lett.* **38**, 157-158 (2002).
58. L.J. Brillson, S.T. Bradley, S.H. Goss, X. Sun, M.J. Murphy, W.J. Schaff, L.F. Eastman, D.C. Look, R.J. Molnar, F.A. Ponce, N. Ikeo, and Y. Sakai, "Low Energy Electron-Excited Nano-Luminescence Studies of GaN and Related Materials," *Applied Surface Science*, vol. 190 498-5077 (2002).
59. G.H. Jessen, B.D. White, S.T. Bradley, P.E. Smith, L.J. Brillson, J. E. Van Nostrand, R.Fitch, G.D. Via, J.K. Gillespie, R.W. Dettmer and J.S. Sewell, "Ohmic Contact Characterization of AlGaN/GaN Device Layers with Spatially Localized LEEN Spectroscopy," *Solid State Electronics*, vol. 46, 1427-1431 (2002).
60. X.L. Sun, S.H. Goss, L.J.Brillson, D.C. Look, and R.J. Molnar, "Electronic Defect States Observed by Cathodoluminescence Spectroscopy at GaN/Sapphire Interfaces," *Physica Status Solidi (b)*, vol. 228, 441-444 (2002).
61. X. L. Sun, S. H. Goss, L. J. Brillson, D.C. Look, and R.J. Molnar, "Depth-Dependent Investigation of Defects and Impurity Doping in GaN/sapphire Using Scanning Electron Microscopy and Cathodoluminescence Spectroscopy," *Journal of Applied Physics*, vol. 91, 6729-6738 (2002).
62. L. W. Massengill, B. K. Choi, D. M. Fleetwood, R. D. Schrimpf, K. F. Galloway, M. R. Shaneyfelt, T. L. Meisenheimer, P. E. Dodd, J. R. Schwank, Y. M. Lee, R. S. Johnson, G. Lucovsky, "Heavy-Ion-Induced Breakdown in Ultra-Thin Gate Oxides and High-k Dielectrics," *IEEE Trans. Nucl. Sci.* **48**, 1904-1912 (2001). *Meritorious Conference Paper Award, 2001 IEEE Nuclear and Space Radiation Effects Conference.*

63. S. N. Rashkeev, D. M. Fleetwood, R. D. Schrimpf, and S. T. Pantelides, "Proton-Induced Defect Generation at the Si-SiO₂ Interface," *IEEE Trans. Nucl. Sci.* **48**, 2086-2092 (2001).
64. A. P. Karmarkar, B. K. Choi, R. D. Schrimpf, D.M. Fleetwood, "Aging and Baking Effects on the Radiation Hardness of MOS Capacitors," *IEEE Trans. Nucl. Sci.* **48**, 2158-2163 (2001).
65. S. N. Rashkeev, D. M. Fleetwood, R. D. Schrimpf, and S. T. Pantelides, "Defect Generation by Hydrogen at the Si-SiO₂ Interface," *Phys. Rev. Lett.* **87**, 165506-1 to 165506-4 (2001).
66. L.J. Brillson, A.P. Young, G.H. Jessen, T.M. Levin, S.T. Bradley, S.H. Goss, and J. Bae, "Low Energy Electron-Excited Nano-Luminescence Spectroscopy of GaN Surfaces and Interfaces," *Applied Surface Science*,. vol. 175-176, 442-449 (2001).
67. L.J.Brillson, "Nanoscale Luminescence Spectroscopy of Defects at Buried Interfaces and Ultra-Thin Films," *Journal of Vacuum Science and Technology*, vol. B19, 1762-1768 (2001).
68. S. T. Pantelides, S. N. Rashkeev, R. Buczko, D. M. Fleetwood, and R. D. Schrimpf, "Reactions of Hydrogen with Si-SiO₂ Interfaces," *IEEE Trans. Nucl. Sci.* **47**, 2262-2268 (2000).
69. P. E. Bunson, M. Di Ventra, S. T. Pantelides, D. M. Fleetwood, and R. D. Schrimpf, "Hydrogen-Related Defects in Irradiated SiO₂," *IEEE Trans. Nucl. Sci.* **47**, 2289-2296 (2000).
70. B. D. White, L. J. Brillson, S. C. Lee, D. M. Fleetwood, R. D. Schrimpf, S. T. Pantelides, Y. M. Lee, and G. Lucovsky, "Low Energy Electron-Excited Nanoscale Luminescence: A Tool to Detect Trap Activation by Ionizing Radiation," *IEEE Trans. Nucl. Sci.* **47**, 2276-2280 (2000).
71. C. J. Nicklaw, M. P. Pagey, S. T. Pantelides, D. M. Fleetwood, R. D. Schrimpf, K. F. Galloway, J. E. Wittig, B. M. Howard, E. Taw, W. H. McNeil, and J. F. Conley, Jr., "Defects and Nanocrystals Generated by Si Implantation into SiO₂," *IEEE Trans. Nucl. Sci.* **47**, 2269-2275 (2000).
72. S. C. Lee, A. Raparla, Y. F. Li, G. Gasiot, R. D. Schrimpf, D. M. Fleetwood, K. F. Galloway, M. Featherby, and D. Johnson, "Total Dose Effects in Composite Nitride-Oxide Films," *IEEE Trans. Nucl. Sci.* **47**, 2297-2304 (2000).
73. Z. Marka, S. K. Singh, W. Wang, S. C. Lee, J. Kavich, B. Glebov, S. N. Rashkeev, A. P. Karmarkar, R. G. Albright, S. T. Pantelides, R. D. Schrimpf, D. M. Fleetwood, and N. H. Tolk, "Characterization of X-ray Radiation Damage in Si/SiO₂ Structures Using Second-Harmonic Generation," *IEEE Trans. Nucl. Sci.* **47**, 2256-2261 (2000).

74. S. C. Lee, Y. F. Zhao, R. D. Schrimpf, M. A. Neifeld, and K. F. Galloway, "Comparison of lifetime and threshold current damage factors for multi-quantum well GaAs/GaAlAs laser diodes irradiated at different proton energies," IEEE Transactions on Nuclear Science, Vol.46, pp.1797-1803, December, 1999.

6 INTERACTIONS/TRANSITIONS

Throughout this program, we worked closely with Umesh Mishra and his team from the University of California-Santa Barbara. They provided many samples for radiation characterization and were an integral team member.

Joe Tringe and John Merrill of Kirtland AFB provided CIGS test structures and solar cells for radiation testing by LEEN and micro-cathodoluminescence spectroscopy at Ohio State University.

We worked closely with Sandia Labs on characterization of total-dose and single-event effects in alternative dielectrics.

Art Edwards of Kirtland AFB collaborated with Ohio State University on deep level calculations of oxygen in high aluminum content AlGa_N.

Ross Dettmer of AFRL provided packaging for the GaN/AlGa_N/GaN devices studied at Vanderbilt University.

We are collaborating with SOITEC and MEMC on application of second harmonic generation to characterization of SOI-wafer interfacial quality.

Vanderbilt University launched the Institute for Space and Defense Electronics (ISDE) to promote application of radiation effects-related research to practical problems of importance to U.S. government programs, laboratories, and contractors. ISDE has a staff of full-time engineers dedicated to performing radiation-effects analysis, modeling, and design activities.

7 NEW DISCOVERIES, INVENTIONS OR PATENT DISCLOSURES

U.S. CIP Patent Disclosure: "Apparatus and Methods of Using Second Harmonic Generation as an Non-Invasive Optical Probe for Interface Properties in Layered Structures," Michael Lee Alles, Norman Tolk, Bongim Jun, Robert Pasternak, Ron Schrimpf, and Sorin Cristoloveanu.

8 HONORS/AWARDS

Leonard J. Brillson, elected IEEE Fellow (2000).

Lloyd W. Massengill, elected IEEE Fellow (2005).

Ronald D. Schrimpf, elected IEEE Fellow (2000).

Leonard J. Brillson, Technical Achievement Award, IEEE Columbus Section (2000).

Leonard J. Brillson, Ohio State University Mortar Board National Senior Honor Society Recognition (2000).

Leonard J. Brillson, Ohio State University Lumley Research Award (2001).

Daniel Fleetwood, Sokrates Pantelides, and Ronald Schrimpf received the Vanderbilt University Chancellor's Award for Research (2003).

Leonard J. Brillson, Office of Naval Research Outstanding Speaker Award (2001).

Leonard J. Brillson, elected Fellow, American Association for the Advancement of Science (2002).

Shawn Bradley, graduate student in Prof. Brillson's Ohio State group won a Best Student Presentation award by the International Semiconductor Device Research Symposium in Washington, DC on Dec. 12, 2004 for his presentation entitled "Dependence of Schottky Barrier Height on Electronic and Chemical Properties of Ni/AlGaN Contacts."

Hao Xiong, a graduate student at Vanderbilt, received the IEEE Nuclear and Plasma Sciences Society Graduate Fellowship and the Phelps Award.

The following paper was selected for the Meritorious Conference Paper Award for the 2001 IEEE Nuclear and Space Radiation Effects Conference:

L. W. Massengill, B. K. Choi, D. M. Fleetwood, R. D. Schrimpf, K. F. Galloway, M. R. Shaneyfelt, T. L. Meisenheimer, P.E. Dodd, J. R. Schwank, Y. M. Lee, R. S. Johnson, G. Lucovsky, "Heavy-Ion-Induced Breakdown in Ultra-Thin Gate Oxides and High-k Dielectrics," IEEE Trans. Nucl. Sci. **48**, 1904-1912 (2001).

The following paper was selected for the Meritorious Conference Paper Award for the 2002 IEEE Nuclear and Space Radiation Effects Conference:

S.N.Rashkeev, D.M.Fleetwood, R.D.Schrimpf, and S.T.Pantelides. Radiation-Induced Acceptor Deactivation in Bipolar Devices: Effects of Electric Field and Irradiation Temperature. Appl. Phys. Lett. **83**, N 22, 4646-4648 (2003).

The following paper was selected for the Meritorious Conference Paper Award for the 2002 IEEE Nuclear and Space Radiation Effects Conference:

S. N. Rashkeev, C. R. Cirba, D. M. Fleetwood, R. D. Schrimpf, S. C. Witzak, A. Michez, and S. T. Pantelides, "Physical Model for Enhanced Interface-Trap Formation at Low Dose Rates," IEEE Trans. Nucl. Sci. **49**, 2650-2655 (2002).

The following paper was selected for the Meritorious Conference Paper Award for the 2002 IEEE Nuclear and Space Radiation Effects Conference:

D. M. Fleetwood, H. D. Xiong, Z. Y. Lu, C. J. Nicklaw, J. A. Felix, R. D. Schrimpf, and S. T. Pantelides, "Unified Model of Hole Trapping, $1/f$ Noise, and Thermally Stimulated Current in MOS Devices," IEEE Trans. Nucl. Sci. **49**, 2674-2683 (2002).

The following paper was selected as the Meritorious Paper for the 2004 Hardened Electronics and Radiation Technology Conference:

R. A. Weller, R. D. Schrimpf, R. A. Reed, A. L. Sternberg, A. S. Kobayashi, M. H. Mendenhall, L. W. Massengill, and D. M. Fleetwood, "Modeling Semiconductor Device Response Using Detailed Radiation Event Simulations."